NAVAL POSTGRADUATE SCHOOL
Monterey, California

THESIS

HEAT FLUXES ASSOCIATED WITH INTRUSIONS DURING THE SHEBA ICE STATION DRIFT

by

Douglas Rogers Lamb

September 2000

Thesis Advisor: Timothy P. Stanton
Second Reader: Robert H. Bourke

Approved for public release; distribution is unlimited.

REPORT DOCUMENTATION PAGE

Form Approved
OMB No. 0704-0188

1. AGENCY USE ONLY *(Leave blank)*	2. REPORT DATE	3. REPORT TYPE AND DATES COVERED
	September 2000	Master's Thesis

4. TITLE AND SUBTITLE
Heat Fluxes Associated with Intrusions during the SHEBA Ice Station Drift

5. FUNDING NUMBERS
OPP-9701391

6. AUTHOR(S)
Lamb, Douglas Rogers

7. PERFORMING ORGANIZATION NAME(S) AND ADDRESS(ES)
Naval Postgraduate School
Monterey, CA 93943-5000

8. PERFORMING ORGANIZATION REPORT NUMBER

9. SPONSORING / MONITORING AGENCY NAME(S) AND ADDRESS(ES)
National Science Foundation
Office of Polar Programs
4201 Wilson Blvd
Arlington, VA, 22230

10. SPONSORING / MONITORING AGENCY REPORT NUMBER

11. SUPPLEMENTARY NOTES
The views expressed in this thesis are those of the author and do not reflect the official policy or position of the Department of Defense or the U.S. Government.

12a. DISTRIBUTION / AVAILABILITY STATEMENT
Approved for public release; distribution is unlimited.

12b. DISTRIBUTION CODE

13. ABSTRACT *(maximum 200 words)*

A yearlong set of temperature and salinity profiles from the Surface Heat Budget of the Arctic (SHEBA) is analyzed to identify intrusions from the mixed layer to a depth of 150 m. Ensemble averaged temperature and salinity profiles, spectral analysis of the vertical thermal structure, and bathymetry are used to divide the SHEBA ice stationtrack into four regions: Beaufort Sea; Northwind Rise and break; Chukchi Plateau and break; Mendelev Abyssal Plain. Average vertical gradients of temperature and salinity over intrusive features are used to calculate Turner angles and molecular heat fluxes. Bering Sea Summer Water dominates the structure in the temperature and salinity profiles of the Northwind Rise region, with a maximum temperature intrusion of 2.2°C. Cold intrusions penetrate the upper halocline in the Chukchi Plateau region. The width of the distribution of Turner angle in the vertical profiles is indicative of the degree of the interleaved structure. Mesoscale features and associated internal wave activity accompany highly variable vertical structure over the Northwind Rise and Chukchi Plateau regions. The role of intrusions in lateral mixing and lateral heat transport is discussed in context of the observed regional differences in water mass properties.

14. SUBJECT TERMS	15. NUMBER OF PAGES
SHEBA, Intrusions, Heat Fluxes, Halocline, Double-diffusion, Turner angle	84
	16. PRICE CODE

17. SECURITY CLASSIFICATION OF REPORT	18. SECURITY CLASSIFICATION OF THIS PAGE	19. SECURITY CLASSIFI- CATION OF ABSTRACT	20. LIMITATION OF ABSTRACT
Unclassified	Unclassified	Unclassified	UL

NSN 7540-01-280-5500

Standard Form 298 (Rev. 2-89)
Pescribed by ANSI Std. 239-18

THIS PAGE INTENTIONALLY LEFT BLANK

Approved for public release; distribution is unlimited

HEAT FLUXES ASSOCIATED WITH INTRUSIONS DURING THE SHEBA ICE STATION DRIFT

Douglas Rogers Lamb
Lieutenant, United States Navy
B.S., United States Naval Academy, Annapolis Maryland, 1992

Submitted in partial fulfillment of the
requirements for the degree of

MASTER OF SCIENCE IN METEOROLOGY AND PHYSICAL OCEANOGRAPHY

from the

NAVAL POSTGRADUATE SCHOOL
September 2000

Author: 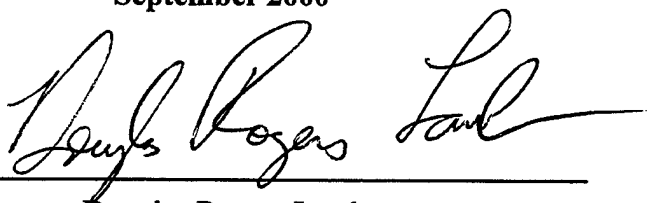

Douglas Rogers Lamb

Approved by: 

Timothy P. Stanton, Thesis Advisor

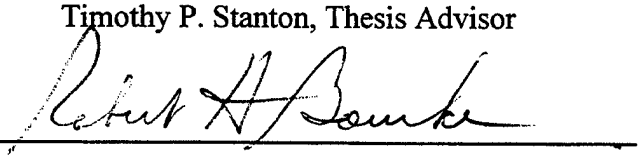

Robert H. Bourke, Second Reader

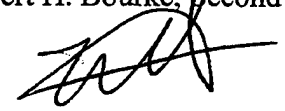

Roland W. Garwood, Chairman
Department of Oceanography

THIS PAGE INTENTIONALLY LEFT BLANK

ABSTRACT

A yearlong set of temperature and salinity profiles from the Surface Heat Budget of the Arctic (SHEBA) is analyzed to identify intrusions from the mixed layer to a depth of 150 m. Ensemble averaged temperature and salinity profiles, spectral analysis of the vertical thermal structure, and bathymetry are used to divide the SHEBA ice station track into four regions: Beaufort Sea; Northwind Rise and break; Chukchi Plateau and break; Mendelev Abyssal Plain. Average vertical gradients of temperature and salinity over intrusive features are used to calculate Turner angles and molecular heat fluxes. Bering Sea Summer Water dominates the structure in the temperature and salinity profiles of the Northwind Rise region, with a maximum temperature intrusion of 2.2 °C. Cold intrusions penetrate the upper halocline in the Chukchi Plateau region. The width of the distribution of Turner angle in the vertical profiles is indicative of the degree of the interleaved structure. Mesoscale features and associated internal wave activity accompany highly variable vertical structure over the Northwind Rise and Chukchi Plateau regions. The role of intrusions in lateral mixing and lateral heat transport is discussed in context of the observed regional differences in water mass properties.

THIS PAGE INTENIONALLY LEFT BLANK

TABLE OF CONTENTS

THIS PAGE INTENIONALLY LEFT BLANK

ACKNOWLEDGEMENT

Dr. Tim Stanton, my advisor, provided direction to my research efforts and insight into the physical processes. I thank Dr Robert Bourke for his valuable criticism and sharing his experience gained from a career in polar oceanography. Both were essential to the completion of this study. Jim Stockell provided much needed assistance in programming and technical support. I also thank Damon Dixon for being a step ahead of me in the thesis processes and helping me avoid potential problems.

Most of all, I thank my family. Erika, my wife and best friend, gave me endless support and encouragement and shared both my enthusiasm and frustrations. Derek, who came into the world during my thesis research, constantly provides joy and perspective. The other members of my family scattered around California have all helped in their own way.

THIS PAGE INTENIONALLY LEFT BLANK

I. INTRODUCTION

Coupled atmosphere/ice/ocean physical processes increase the sensitivity of polar regions to climate change and must be accurately understood and modeled to make future global climate predictions. The Surface Heat Budget of the Arctic Ocean (SHEBA) is an interdisciplinary observation and modeling program designed to study the physical processes and associated feedback mechanisms that govern the Arctic ice pack. To achieve this goal, the Canadian Coast Guard icebreaker *Des Groseilliers* was frozen in the Arctic icepack between October 2, 1997, and October 11, 1998. The SHEBA ice camp floated from 75° N, 152° W to 80° N, 162° W, while serving as a base of operations to the nearby ice camp and observation systems. In all, the SHEBA ice station traveled over 2800 km with a net displacement of 770 km, as it passed through the Beaufort Sea and over the topography of the Northwind Ridge, Chukchi Plateau and Mendelev Abyssal Plain.

Yearlong time series were collected of the parameters describing the physical state of the environment around the ice station. As part of this data set, over 12,000 upper ocean vertical profiles of temperature and salinity were obtained. These profiles allow near continuous monitoring of the state of the upper pycnocline. Since the pycnocline largely isolates the surface from heat contained within the Atlantic layer and maintains the stability of the Arctic ice pack, understanding the flow of heat within the pycnocline is crucial.

The total pycnocline heat flux is composed of three components: molecular heat flux; double diffusive heat flux; and turbulent heat flux. The emphasis within the present

study is on the role of intense intrusions on the order of tens of meters rather than turbulence. Thus, the goals of the study are to develop a technique to estimate the vertical gradients of temperature and salinity in the presence of strong interleaving. The gradients can then be used to estimate molecular and double diffusive heat fluxes, and then identify mechanisms contributing to these fluxes. Next, the regional differences in water mass properties are explored to discover how they contribute to differences in observed temperature profiles in the upper pycnocline. Finally, the life spans of the intrusions are empirically quantified.

II. BACKGROUND

A. CIRCULATION AND WATER MASSES OF THE ARCTIC OCEAN

The Canadian Basin of the Arctic Ocean is divided into the Canada and Makarov Basins by the Alpha-Mendelev Ridge. The Beaufort Sea, with a maximum depth of 3800 m, lies within the southern Canada Basin. Surrounding the Canada Basin are several shallow seas: the Chukchi Sea with a depth on the order of 50 m; the southern portion of the Beaufort Sea with a depth on the order of 50 m; the East Siberian Sea with depths of 20 – 40 m. The continental shelf along Alaska and the Canadian Archipelago, which is less than 50 km wide, is relatively narrow, but the shelf along Siberia typically extends seaward 600 – 800 km. The bathymetric slope of the Canadian Basin is gradual towards Amundsen Gulf and Mackenzie Bay, but steepens towards the Alaskan and Chukchi Shelves. The Chukchi Plateau and Northwind Rise are topographic features at the Pacific end of the Canadian basin, between the Beaufort Sea and the Chukchi Sea with depths of approximately 500 m and 1000 m, respectively. These features have extremely steep eastern slopes. To the north of the Chukchi Plateau lies the Mendelev Abyssal Plain (*Carmack*, 1990) (Figure 1).

The Arctic surface circulation has historically been described as being forced by the Beaufort high pressure system which is centered over most of the Canadian Basin. The Beaufort High drives the anti-cyclonic Beaufort Gyre and outflow through the Transpolar Drift Stream (*Carmack*, 1990). The Beaufort Gyre causes Ekman convergence and downwelling in the Canada Basin, which depresses the halocline. Evidence accumulated through the 1990's has revealed that the atmospheric high

pressure cell has become weaker and centered over western longitudes (*Walsh et al.*, 1996). This shift in the atmospheric system may have caused the circulation of the Beaufort Gyre to become weaker and be limited to the Canada Basin. Two oscillating climatological states, anticyclonic and cyclonic, have been proposed to represent these circulation patterns, with each regime lasting 5 –7 years (*Proshutinsky et al.*, 1998). The Arctic climate was in the anticyclonic regime during 1972 – 1979 and 1984 –1988. The cyclonic regime dominated during 1980-1983 and 1989 – 1998, the period of the SHEBA experiment. During the anticyclonic periods, the front separating the waters of the European Basin and the Canadian Basin was traditionally located over the Lomonosov Ridge, but during the 1990's cyclonic regime, it has been shifted westward and located over the Alpha Mendelev Ridge (*McLaughlin et al.*, 1996). One consequence of the atmospheric shift during the 1990s is that a branch of the warm, saline flow from the European Basin followed the continental shelf and migrated into the Chukchi Sea (*McLaughlin et al.*, 1996).

Pacific inflow through Bering Strait connects the waters of the Bering Sea with those of the Chukchi Sea. The long-term mean transport is approximately 0.8 Sv to the north, but an annual transport cycle with an amplitude of 0.6 Sv has been observed (*Roach et al.,* 1995). The flow is higher in summer than in winter. The Pacific inflow bifurcates upon entering the Chukchi Sea with the two primary branches directed towards Herald Canyon and Barrow Canyon (Figure 2). The water mass characteristics of the inflow are representative of nutrient–rich Gulf of Anadyr water, fresher Alaskan Coastal Water, and Bering Sea Water (*Coachman et al.*, 1974). Shelf processes further modify the characteristics (*McLaughlin et al.*, 1996). In the Beaufort Sea, water of Pacific origin

can be identified by its temperature and salinity characteristics. Pacific Water with a T_{max} at $31<S<32$ and a T_{min} at S ~33.1 is classified as Bering Sea Summer Water (BSSW) and Bering Sea Winter Water (BSWW), respectively (*Coachman et al.*, 1974; *Jones et al.*, 1990). (All salinities in this thesis are in practical salinity units, psu.)

The vertical temperature-salinity structure of Arctic Ocean waters is divided into three main layers: the surface layer, the intermediate or Atlantic layer, and the deep water (*Carmack*, 1990). Since SHEBA is a surface process study located in the western Arctic, only the surface layer of the Canada Basin will be discussed in detail. The surface layer is divided into the mixed layer and the upper halocline (also known as the cold halocline) (*Jones et al.*, 1990). A lower halocline may be present in parts of the Canada Basin. The Arctic mixed layer is the result of winter convective activity and typically extends to 20 – 50 m. The temperature is isothermal and near freezing year-round. The salinity is isohaline, but the value varies widely from 26 – 34 due to the annual ice cycle. The upper halocline lies typically between 20 m and 120 m and is characterized by upper halocline water (UHW), which is less than –1 °C with $33.1<S<33.5$. The UHW may contain a temperature maximum near S ~32, representative of BSSW (*Carmack*, 1990). Data from the Scientific Ice Expedition (SCICEX), oceanographic cruises aboard U.S. Navy nuclear submarines, suggest that during the cyclonic regime of the 1990s the UHW has retreated from the Eurasian Basin and is found only in the Canadian Basin (*Steel and Boyd*, 1998). Beneath the UHW is the lower halocline water (LHW), which warms slowly from 150 m to the core of the Atlantic layer at approximately 400 m and becomes more saline. The salinity of the LHW is in the range of $33.1<S<34.4$ (*McLaughlin et al.*, 1996).

The seasonal ice melt and the resultant fresh water input at the surface forms the halocline (*Carmack*, 1990). Because the temperature remains low within the halocline, the UHW cannot be a simple mixture of surface waters (cold and fresh) with Atlantic layer waters (warm and salty). Processes that modify the water mass properties are required to maintain the upper halocline. The UHW in the Canadian Basin is maintained by the lateral shelf drainage of near freezing, high salinity intrusions and the mixing of upwelled Atlantic intermediate water with cold, fresh summer shelf water (*Aagaard et al.*, 1981). The source of the intrusions is primarily Bering Sea Water (BSW), modified by the freezing process and storm passage (*Melling and Lewis*, 1982). Because salinity depresses the freezing point, salinity greater than S = 24.7 causes the freezing point to be greater than the temperature of maximum density. Surface cooling of a water mass of sufficient salinity creates a vertical instability and convective mixing results. This continues until the entire water mass reaches the freezing point. Continued surface cooling ultimately results in freezing of surface waters. Because a weak vertical density gradient typically exists over the shallow Beaufort and Chukchi shelves, the entire water mass upon the shelf is cooled in this manner. The freezing process injects brine into the near surface water, increasing its density. This water mass then slowly sinks or is turbulently mixed by a passing atmospheric storm. Once sufficiently saline to penetrate the halocline, the modified water mass slides off the shelf into deeper water. The dependence on storms and the intensity of the freezing process causes the volume flow and water mass properties of the intrusions to be highly variable.

B. HISTORIC WATER MASS PROPERTIES

Historic temperature and salinity values, representative of the geographic regions traversed by the SHEBA ice station, were obtained from the Environmental Working Group (EWG) summer and winter climatological atlases. These atlases consolidate Arctic data worldwide, including Russian data and declassified U.S. Navy data which was previously unavailable. The EWG data are depicted as decadal means for 200 km by 200 km grids and at specific depth intervals; grids corresponding to the SHEBA track are analyzed. The values obtained are estimated from the analysis of *Tyner* (1999). In order to maintain seasonal and geographical comparisons, March – May mean data was compared with the SHEBA data when the ice station drifted in the western Beaufort and over the Chukchi Plateau during the fall and early winter. The use of late winter / early spring data was necessitated by the depth of historical mid-winter data for this region. July – September data was used for comparison when the SHEBA camp drifted across the Chukchi Plateau and Mendelev Abyssal Plain. The decadal EWG averages were constructed prior to widespread awareness of the separate states (i.e., cyclonic and anticyclonic regimes) of the Arctic Oscillation.

The historic mixed layer in the western Beaufort Sea and Chukchi Plateau regions is freshest and warmest from March - May. During July - September, the mixed layer over the Chukchi Plateau is the warmest, while the Mendelev Abyssal Plain mixed layer remains near freezing during spring and summer because of the thicker permanent ice pack.

The March to May 50 m mean temperatures were warmest in the western Beaufort Sea and Chukchi Plateau, ranging from –1.61 °C to –1.08 °C. The freshest

water at 50 m was in the western Beaufort Sea, and the most saline was in the Chukchi Sea. The March - May high salinity in the shallow Chukchi Sea and the fresher water in the deeper Beaufort Sea are supportive of the concept of dense water formation and the flow of saline BSW across the Chukchi Sea into the Beaufort Sea. The July to September mean temperature at 50 m is warmest over the Chukchi Plateau, while the Mendelev Plain remains almost isothermal to 50 m, with the mean temperature near freezing. The 50 m mean salinity over the Chukchi Plateau was approximately equal to that over the Mendelev Abyssal Plain, but the gradient at the former was much stronger.

At 100 m from March to May, the warmest and freshest water was in the western Beaufort Sea at –1.3 °C and 32.2<S<32.7. Over the Chukchi Plateau, the mean temperature and mean salinity were –1.4 °C and 32.4<S<32.7, respectively. The July to September mean temperature at 100 m varied from –1.6 °C to –1.1 °C across the Canada Basin, and the mean salinity varied little from 32.1<S<32.8.

The 1993 SCICEX cruise of the U.S.S. *Pargo* transited the Chukchi Plateau in August of 1993 and conducted CTD casts. The following data, representative of conditions during the cyclonic regime, were estimated from *Morison et al.* (1998) (Figure 3). The surface temperature was ~-1.6<T<-1.5 and the surface salinity was 30<S<31. The salinity at 50 m was 32, and at 100 m was 33.

C. STABILITY AND DOUBLE DIFFUSION

In regimes where the ocean temperature is near freezing, the thermal expansion coefficient (defined as $\alpha = -\rho^{-1} (\partial\rho / \partial\theta) \approx 10^{-5}$) is an order of magnitude less than the haline contraction coefficient (defined as $\beta = \rho^{-1} (\partial\rho / \partial S) \approx 10^{-4}$) (*Gill*, 1982).

Consequently, density is determined primarily by salinity, and temperature can often be approximated as passive water mass tracer. Thus, the pycnocline closely follows the halocline, even in the presence of strong thermal intrusions.

Double diffusion is a physical process in which vertical fluxes are driven by the different rates of molecular diffusion of two properties; for oceanic cases, the two properties are salt and heat (*Turner*, 1995). The molecular rate of diffusion of heat is 100 times greater than for salt. For double diffusion to occur, the diffusing components must have opposing effects on the vertical density gradient. This requires the vertical thermal and salinity gradients, T_z and S_z, to have the same sign. As a result of double diffusion, the potential energy of the system always decreases; therefore, the magnitude of the vertical density gradient increases (*Turner*, 1995). This is the opposite of a turbulent mixing process.

If the energy for double diffusion comes from the component with the larger diffusivity, T_z and S_z must be negative (where z is positive up throughout), and diffusive convection may occur (*Turner*, 1995). This describes a system with a stable salinity gradient heated from the bottom, which was the dominant situation in the regions examined by this study. In the regions traversed by SHEBA, the salinity gradient was almost always negative, and diffusive convection was the dominant mechanism in regions where the interleaved structure provided negative thermal gradients. In diffusive convection, the vertical diffusion of heat upward across an interface creates a convectively unstable layer that can separate when it overcomes the viscous forces. Convection is sustained by the more rapid diffusion of heat relative to salt across this diffusive interface.

If T_z and S_z are positive (with z positive up), the energy comes from salt diffusion, leading to the process called salt fingering (*Turner*, 1995). In this situation, the more rapid diffusion of heat relative to salt downward across an interface causes a parcel on the interface to bow upwards due to the thermally decreased density. As the heat diffuses out of the adjacent parcel, it is left cooler with a higher salinity and denser than the surrounding water. As the double diffusion continues, long, narrow convective cells are formed, sustained by the more rapid sideways diffusion of heat (*Turner*, 1995).

A parameter introduced that describes the strength of double diffusion is the Turner angle, Tu (*Ruddick*, 1983):

$$Tu = \tan^{-1}\left(\frac{\alpha T_z + \beta S_z}{\alpha T_z - \beta S_z}\right) \qquad \text{Eq. 1}$$

where the $\tan^{-1}$ is the four quadrant inverse tangent. Table 1 shows the possible values of Tu and the respective double diffusive processes.

$-90° < Tu < 0°$	Diffusive Convection
$-45° < Tu < 45°$	Hydrostatically Stable
$45° < Tu < 90°$	Salt Fingers
$Tu < -90°$ or $90° < Tu$	Hydrostatically Unstable

Table 1. Turner angle and double diffusive regimes.

Examination of Eq. 1 reveals why the diffusive convection regime is expected in polar regions. In cold waters, β is an order of magnitude larger than α, with β being positive and α being negative. Because the magnitude of αT_z is much less than βS_z, the argument

of the inverse tangent will typically fluctuate around –1, and the Turner angle will fluctuate around –45°. Thus the water column will be hydrostatically stable or have weak diffusive convection. Even in a region where T_z and S_z are both negative (i.e., temperature and salinity increase with depth), T_z must be sufficiently larger than S_z to compensate for the dominance of β, in order to generate strong diffusive convection.

D. DOUBLE DIFFUSION AND INTRUSIONS

An intrusion is identified as a T-S anomaly relative to the mean state (*Robertson et al.*, 1995). The interaction between double diffusion and intrusions has been observed in both laboratory experiments and theoretical models. The intrusions provide the necessary thermal and salinity gradients; double diffusion supplies a driving force to modify the shape and water properties of the intrusions (*Turner*, 1978; *Toole and Georgi*, 1981). As warm, salty water intrudes into cool, fresh water along a given isopycnal, the cool, fresh water is displaced vertically, above and below the intrusion. This is the case as BSW enters the Beaufort Sea. At the top boundary of the intrusion, diffusive convection across the boundary causes the cool, fresh water to become warmer and less dense. The warm, salty water loses heat and becomes denser. At the lower boundary, heat also flows out of intrusion. Consequently, the intrusion experiences a net positive density flux (i.e., becomes denser), and, with a sufficiently large time scale, will slope downward across the isopycnals. The resultant density anomaly and the layer slope establish a pressure gradient anomaly that drives along-layer advection (*Ruddick and Walsh*, 1995). The lateral mixing process associated with Atlantic layer intrusions in the

Arctic Ocean has been shown to facilitate material transport from the topographically steered boundary currents into the basin interior (Carmack et al., 1997).

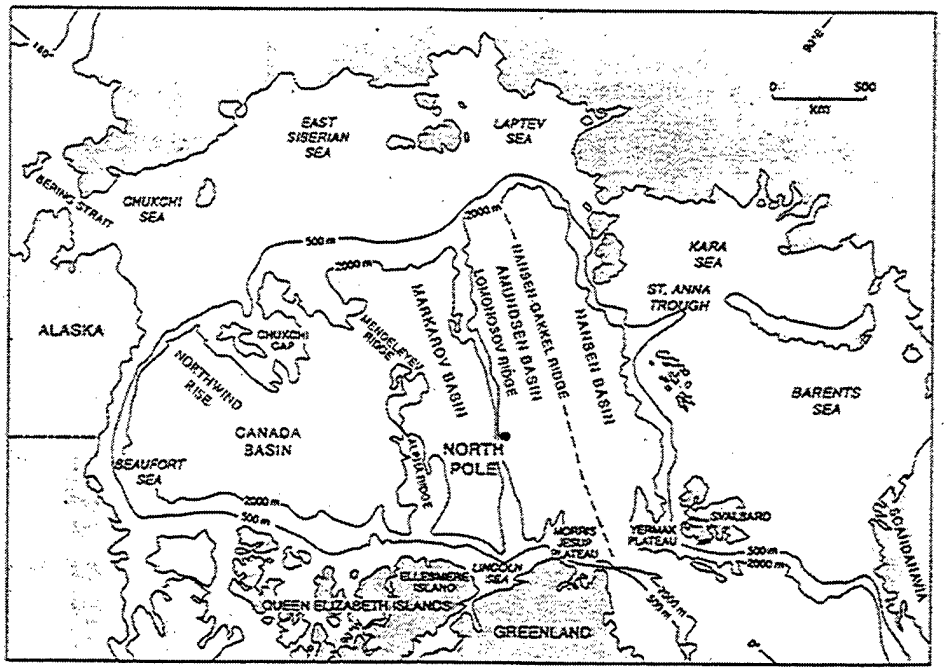

a)

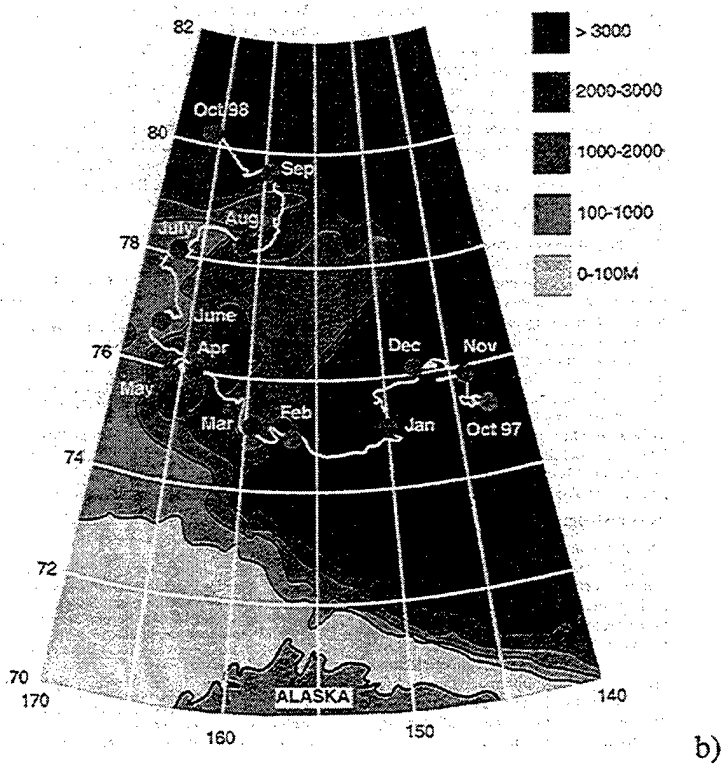

b)

Figure 1. a) The Arctic Ocean (After *Anderson*, 1995). b) The SHEBA ice station drift track (From *Perovich et al.*, 1999). Bathymetric contours in meters.

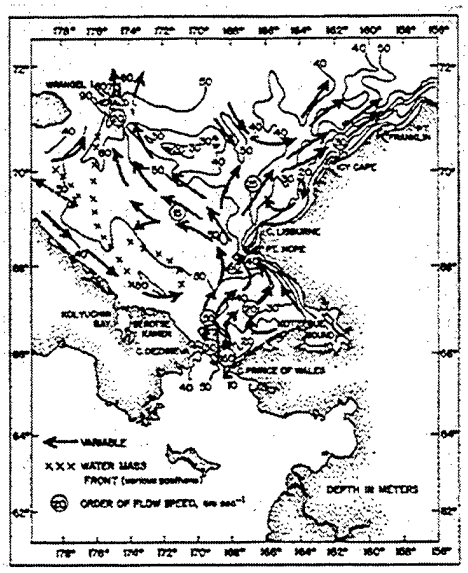

Figure 2. The flow through Bering Strait (*From Coachman et al.*, 1975).

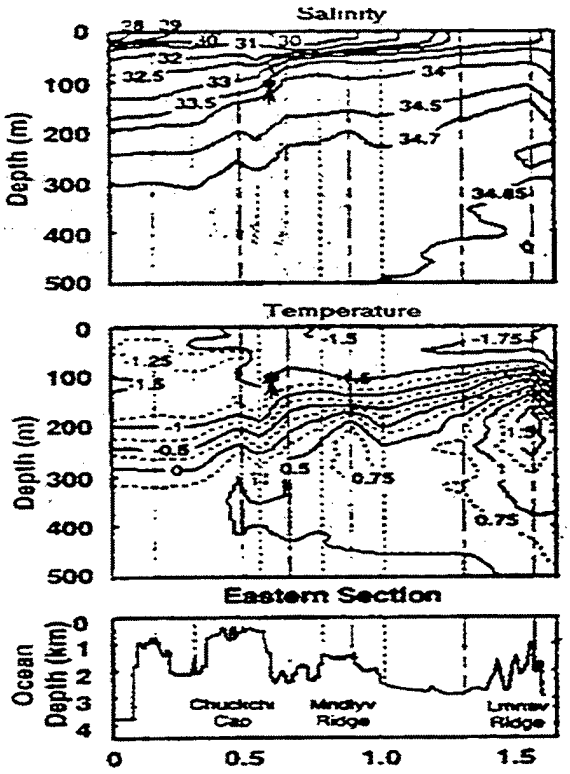

Figure 3. Temperature contours, salinity contours, and bathymetry from the eastern section of the SCICEX 93 cruise of the *U.S.S. Pargo*. Abscissa is distance from CTD station closest to Alaska (km) (After Morison et al., 1998).

III. INSTUMENTS AND METHODS

A CTD was deployed far enough from the *Des Groseilliers* to avoid the ship's motion and discharges from disrupting the mixed layer or creating thermal contamination. The CTD automatically cycled between approximately 4 m and 150 m with a ten minute turnaround cycle (*Stanton et al.*, 2000). The Sea Bird 911+ CTD was sampled at 24 Hz and equipped with dual temperature (T) and conductivity (C) sensors, a Sea Tech transmissometer, and a thermal microstructure package. The redundant T and C sensors were changed with recently calibrated sensors four times throughout the year. The initial system run time was two to four hours per day, but it was often extended when interesting features were observed in the real time display. Later in the time series, the profiling was increased to six to twenty-four hours per day. During post processing, the raw, digitized time series were calibrated, and the conductivity and temperature were lagged by one sample interval to minimize salinity spiking before the computation of salinity (S). The resulting T, C, and S values were binned into 10 cm depth increments. An interactive, graphical screening program identified the differences between the profiles from each sensor pair, in order to select the best sensor pair for the remaining analysis. Over 12000 profiles were obtained from SHEBA, with usable resolutions of $< 1 \times 10^{-3}$ °C and < 0.001 psu salinity, and absolute accuracies of approximately 2×10^{-3} °C and 0.004 psu based on post-calibrations.

Because the ice station was subjected to wind forcing, neither pure Lagrangian nor Eularian measurements were possible. Changes in the vertical structure could not be classified solely as changes due to temporal or spatial evolution. Therefore, in the

analysis of the data, three questions continuously determined the methodology: How are temporal verses spatial variations isolated? How are seasonal verses regional effects isolated? What temporal and spatial scales highlight trends or differences in the data?

Although the *Des Groseilliers* was frozen in the icepack on October 2, 1997, for the purposes of this study, the full data set refers to the data collected between yeardays 97330 to 98270, corresponding to November 26, 1997 to September 27, 1998. The data after yearday 97330 contained consistently cleaner data sampled on a more frequent basis.

The first step in the data analysis was the examination of the data set in its entirety. For each yearday, all of the temperature, salinity and derived sigma-t profiles were ensemble averaged. In the analysis of the full data set, only the data between 10 m and 120 m were examined. These upper and lower bounds were selected because the upper 10 m was always above the main thermocline and the upper halocline, and the majority of the thermal variance was above 120 m. From the full data set, large-scale trends and fluctuations became apparent. The full data set was then partitioned based on observational differences in order to investigate the time/space series at smaller time scales on the order of hours to days. When the data was analyzed on the smaller time scales, no ensemble averaging was performed; the individual profiles were examined from the surface to 150 m. This provided a more detailed analysis in the context of a given region and season, while showing the actual temporal sampling. It also allowed for the comparison of the measured physical properties that offers the potential to distinguish between phenomena unique to a geographic region.

Spectral analysis provided the distribution of thermal variance with vertical wavenumber and indicated the vertical scale at which physical processes occur. Successive spectra show the evolution of thermal variance during the observation period. The 0.1 m resolution provided a Nyquist wavenumber of 5 m^{-1} (20 cm). The slope of the thermal spectra in the SHEBA data set was approximately –3. In order to emphasize small changes, the spectra were multiplied by the wavenumber cubed, thus removing most of the slope.

A highly intrusive vertical profile is shown in Figure 4. An objective of this study was to determine the temperature gradients in the presence of strong interleaving. Because the gradient contains numerous relative maxima and minima, determining the mean gradient for an intrusive feature requires that an appropriate vertical scale be identified. The predicted vertical wavelengths of intrusions is O(10) m based on previous theoretical work using flux parameterizations in the presence of strong T - S gradients and on empirical evidence from the lateral erosion of eddies by intrusions (*Toole and Georgi*, 1981; *Walsh and Ruddick*, 1995). The temperature profiles were low-pass filtered with a cut off of 0.5 m^{-1}, leaving a minimum resolved wavelength of two meters. The locations where the temperature gradient passed through zero were used to identify the intrusions, and the vertical temperature gradient of the low-passed profiles was calculated. Figure 4 provides an example of an unfiltered profile plotted with a low-passed profile with locations where the gradient equaled zero. The change in temperature across the segment was divided by the change in depth to calculate the "mean temperature gradient" between successive zeros in the low-passed temperature plot. The salinity gradient was calculated using the change in salinity across the same depth values

as the temperature gradient. Although this technique does not calculate the empirical mean, it adequately resolved the intrusions that were repeatedly present from hours to days, and omitted the finest structure that had relatively fleeting lifetimes. The gradient for each segment was placed into one-meter depth bins. In this manner, each profile was divided into segments defined by the locations where the thermal gradient passed through zero and condensed into one-meter bins.

Once the average gradients were obtained, further analysis of the intrusions was possible. The Turner angle was calculated using Eq. 2 for each segment. The heat flux due to molecular diffusion was calculated using the Fourier Flux Law, which states that the molecular conduction, F_m, is proportional to the temperature gradient: $F_m = -k \nabla T$, where k is the thermal conductivity (*Kundu*, 1990). A value at 0 °C and atmospheric pressure of $k = 0.5610$ W m^{-1} $°C^{-1}$ was used throughout (*Lide*, 1997). The Turner angle and molecular heat flux values were stored in their respective one-meter depth bins.

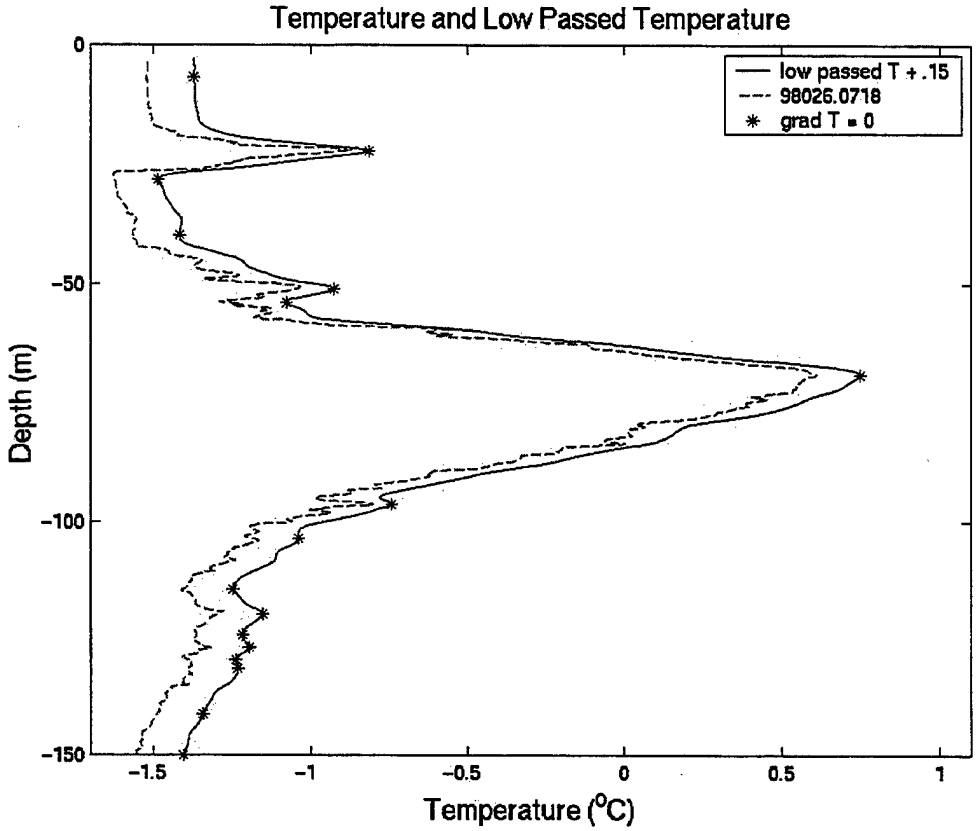

Figure 4. Vertical temperature profile from yearday 98026.07. Also shown is the same profile low-pass filtered at 0.5 m^{-1} shifted right by 0.15 °C for clarity. Asterisks indicate locations in the low-passed profile where the vertical gradient is zero that are used to construct the average gradient over an intrusive feature.

THIS PAGE INTENTIONALLY LEFT BLANK

IV. OBSERVATIONS AND RESULTS

A. FULL DATA SET: DAYS 97330 – 98270

The one-day ensemble averaged temperature time series between 10 m and 120 m is displayed in Figure 5. The temperature within the mixed layer and at 120 m was approximately –1.7 °C, and warmer temperature signals appear as positive deviations from the near freezing temperatures. During December 1997, the thermocline was at ~40 m. The maximum temperature, T_{max} ~ -0.6 °C, at this time was in a layer at 61 m. Around 97355, a second layer became evident at 42 m. In later January, a layer containing significant heat was observed at a depth between 40 and 70 m with an ensemble averaged T_{max} near 0.5 °C. Only a much weaker thermal signal (T_{max} –0.6 °C) remains by day 98100. Between days 98120 and 98170 many thermally unstable layers are evident, where the temperature fluctuates between –1.7 °C and –1 °C. After day 98200, only small temperature signals were observed with small fluctuations between –1.7 °C and –1.4 °C.

Figure 6 shows the one-day ensemble averaged salinity for the full data set. A fresh mixed layer (S ~ 27) extending to ~ 40 m was present until early January, where a transition occurs to a regime where the top of the halocline is above 20 m. The mixed layer salinity increased to S ~ 30.2 by day 98035. The strong thermal signal that was present from 98020 – 98100 between 40 and 70 m occurred with a corresponding salinity of $31 < S < 32$. This intrusion can be classified as Bering Sea Summer Water. From 98070 – 98200, the mixed layer salinity fluctuated between $30.4 < S < 31.9$. After 98200, as the ice station left the plateau and crossed over the Mendelev Abyssal Plain, the mixed

layer depth (MLD) began to deepen, and the salinity dropped to 29.8<S<30.0, possibly due to the seasonal ice melt. The one-day ensemble averaged sigma-t (not shown) exhibited the same features as Figure 6 due to the dominant effect of salinity on density at these low temperatures.

The spectral energy progressively increased as the ice station drifted in the Beaufort Sea to day 98024 (Figure 7). Both axes of the spectra are plotted on a $\log_{10}$ scale, and the mean slope was removed through multiplication by the wave number cubed. The vertical height of each spectrum in the time series is indicative of thermal variance. After the strongest thermal variance period, from 98024 –98027, the variance levels decreased for the remainder of the ice station drift. The maximum spectrum at day 98024 is more than an order of magnitude greater than that observed in the Beaufort Sea, and three orders of magnitude greater than when over the Mendelev Abyssal Plain. The variance was greatest in wavelengths between 1 m and 10 m. The summed variance for wavelengths 1 – 10 m was summed over all spectra (Figure 8, where again the data is plotted on a $\log_{10}$ scale). The greatest variance occurred in January and February, with the maximum on day 98024, nine orders of magnitude above the minimum variance. A slow roll off occurred after day 98060, and then was nearly constant for days 98110 – 98155. After day 98155, as the ice station drifted from the northern slope of the Chukchi Plateau to the Mendelev Abyssal Plain, the variance was near zero, with the exception of a small amount around day 98200.

The high thermal variance on days 98024 – 98027 reflects the strongly interleaved warm water with the temperature spanning –1.5 °C< T < 2 °C. The maximum value of ~2°C was much larger than the T_{max} for any other region, causing the variance to be much

higher. Other regions exhibited interleaved layers, but not with fluctuations of the extreme magnitudes that occurred on days 98024 - 98027. The T_{max} decreased throughout the data set, which would account for the decreasing thermal variance after day 98027.

Figure 9 displays the one-day ensemble-averaged molecular heat flux. Until early January, the upward flux was concentrated in two layers corresponding to the layers with a strong temperature signal at 42 m and 61 m. From day 98025 until 98060, positive heat flux was present above 50 m. The depth of this positive band decreased until 98100 where it reached 30 m. The positive fluxes were then intermittent extending to 40 m. Regions of negative heat fluxes were found below the positive fluxes corresponding to the negative temperature gradient as the temperature decreased to –1.7 °C at 120 m. After day 98150, no significant regions of molecular heat flux appeared in the ensemble-averaged data. The range of values spanned from –0.07 Wm^{-2} to 0.08 Wm^{-2}.

The one-day ensemble-averaged Turner angle (Tu) for the entire data set is shown in Figure 10. Prior to day 98020, vertical layers are present where Tu values possess small fluctuations about –45°. From 98020 – 98100, the layer of warm water from 40 m – 70 m is evident as a region of Tu > -45°, due to the negative temperature gradient. From yearday 98100 – 98165, Tu is highly variable with depth. After day 98200, there are few deviations from Tu of approximately –45°.

Using the one-day ensemble averaged data and considering the changing thermal variance in relation to the bathymetry (Figure 8), the SHEBA data set was divided into 4 regions:

1) Beaufort Sea: 97330<day<98010. The mixed layer depth was ~ -40 m. The thermal variance was more than an order of magnitude less than the peak. The summed variance of wavelengths 1 –10 m was two orders of magnitude less than the peak, with much of it above the mean. The strongest molecular heat flux in this region was divided into two layers at 42 m and 61 m.

2) Northwind Rise and break: 98010<day<98100. A strong thermal signal was seen in the range 40<z<70 m, with T_{max} at 31<S<32. This region showed the strongest BSW signal. The maximum thermal variance occurred in this region as the ice station first encountered the BSW, and remained high until the BSW signal faded. The molecular heat flux was strongest in this region corresponding to the heat contained in the BSW.

3) Chukchi Plateau and break: 98100<day<98220. The roll off of the summed thermal variance between 1 – 10 m became shallower, but still showed significant energy present. The mixed layer salinity was the greatest encountered, 30.6. Frequent vertical and horizontal changes occurred throughout the water column. Both the thermal signal and molecular heat flux decreased throughout this region.

4) Mendelev Abyssal Plain: 98220<day<98270. The temperature of the water column remained –1.7 <T<-1.4 °C as the ice station moved off the plateau and passed over the Chukchi Abyssal Plain. The mixed layer became fresher S~29.8, and the halocline deepened to 35 m. The ensemble data showed little thermal variance or molecular heat flux.

B. REGIONAL REPRESENTATION

The focus of this section shifts from the entire data set to the four regions listed above. Ensemble averaging was performed on only the data for the spectral plots, while the remainder of the data displayed here consists of individual profiles. Figure 11 displays four vertical profiles chosen to represent the four regions: Beaufort Sea, profile 97345.0003; Northwind Rise and break, profile 98024.0011; Chukchi Plateau and break, profile 98144.0353; Mendelev Abyssal Plain, profile 98262.5304. The Northwind Rise profile was chosen when the strong BSW signal was first sampled, which was also the time with the most thermal variance. This choice was motivated in order to examine the changing gradients of the interleaving BSW. The Beaufort Sea profile had a MLD of 40 m and a T_{max} of –0.77 °C at 62 m. A relative T_{max} existed at 44 m. The Northwind Rise MLD was at 28 m and T_{max} was 0.44 °C at 65 m. Many finger-like intrusions were present. The Chukchi Plateau profile had a MLD of 38 m. Many temperature fluctuations between –1.5 °C and –1.2 °C occur down to 120 m. Below 120 m the profile maintained a negative (with z positive up) temperature gradient to 150 m. The mixed layer in the Mendelev Abyssal Plain profile extends to 27 m. A near surface T_{max} of –1.39 °C occurred at 30m. The temperature gradient became negative at 130 m. The main upper haloclines correspond to the thermoclines (Figure 12), but the Northwind Rise and Chukchi Plateau profiles revealed MLD salinity increases of 0.09 at 19 m and 0.05 at 18 m, respectively. The negative temperature gradients in the Chukchi Plateau and Mendelev Abyssal Plain profiles below 120 m and 130 m, respectively, correspond to the lower halocline above the warmer, saltier water of the Atlantic layer.

Figure 13a shows the overlaid T-S plots. Because of the dominant effect of salinity on density at cold temperatures, isopycnals have similar slopes to the isohalines. Temperature spikes, identifying the strong BSSW signal, are evident in the Northwind Rise trace. The multiple spikes between $31<S<32$ are indicative of the interleaved structure as the strong BSSW signal was first observed. The Beaufort Sea, Northwind Rise and Chukchi Plateau plots are similar between $32.3<S<32.9$, where a common water mass may be shared at this depth. The Chukchi Plateau and Abyssal Plain plots slope towards warm salty water at depth, indicative of the lower halocline evident from 120 m -150 m and above the Atlantic layer.

The thermal spectra of the four profiles are displayed in Figure 13b. All four had similar slopes with a value slightly under -3. The slopes of the thermal spectra are the same because similar physical processes occur in each of the different geographic regions. The intensities of the vertical thermal gradients are different, and the vertical wavelengths of intrusions are different, but the processes are similar. Because the thermal intrusions are so much larger over the Northwind Rise, its spectrum is an order of magnitude greater than that of the Beaufort Sea or Chukchi Plateau, and two orders of magnitude greater than that of the Mendelev Abyssal Plain. In Figure 13c, the spectra are multiplied by the wave number cubed. The gentle maxima of all four spectra are at a wavelength of approximately 1 m; however, the Mendelev Abyssal Plain spectrum has a more pronounced maximum because the heat is concentrated in layers on the order of a meter thick. The flatter Northwind Rise spectrum is indicative of thermal variance across a broader band of wavenumbers. Relative minima in the Beaufort Sea, Mendelev

Abyssal Plain, and Northwind Rise are evident, while the Chukchi Plateau still has a negative slope at the cutoff.

Ten-day time series representing the four regions listed above are analyzed below. Ten days were chosen because it was sufficient for the evolution and decay of structure in the vertical profile, while at the same time being longer than synoptic atmospheric events. The yeardays of the respective regions follow: Beaufort Sea, 97345 - 97355; Northwind Rise and break, 98020 - 98030; Chukchi Plateau and break, 98140 - 98150; Mendelev Abyssal Plain, 98260 - 98270. The T-S plots for the ten days representing the Beaufort Sea are displayed in Figure 14a. The ten days were divided into three sections, and each section was plotted with a different symbol. This allowed the evolution of the vertical structure to become apparent. A permanent temperature relative maximum of approximately –0.7 °C existed with salinity between $31<S<32$, corresponding to BSSW. A second temperature relative maximum evolved over the ten days with salinity between $29<S<30$. The permanent relative maximum corresponds to the thermal intrusion at 61 m, and the second corresponds to the T_{max} at 42 m.

The Northwind Rise ten-day T-S diagram, Figure 14b, depicts the growth of the strong temperature signal at salinity between $31<S<32$ consistent with BSSW. An initial $T_{max} \sim -0.4$ °C was present and grew to $T_{max} \sim 2.2$ °C over the ten days. The temperature of the interleaved layers of the Northwind Rise region spanned -1.5 °C $<T<2.2$ °C, a temperature change four times greater than the other regions. The overall temperature spike was composed of many interleaved layers. Concurrently, the upper 40 m of the water column became more saline. As the BSSW intruded on the $\sigma_t \sim 25.8$ isopycnal (S

31.5), the Beaufort Sea water mass above this was displaced upwards, increasing the salinity of the upper water column.

The Chukchi Plateau ten-day T-S evolution possessed the most variability in successive profiles (Figure 14c). A feature with a $T_{max} \sim -0.95$ °C at S ~ 31.7 decayed, while a relative temperature maximum at T ~ -1.1 grew and decayed over four days (a drift of ~30 km). Many temperature fluctuations occurred at a salinity of S ~ 32.5. This is indicative of horizontal variation in water masses. Individual profiles revealed an interleaved structure. A cold water intrusion penetrated at S ~33, and the temperature in the lower halocline decreased.

The Mendelev Abyssal Plain T-S diagram, shown in Figure 14d, shows the decay of a temperature relative maximum at S ~31.3 and some transient signals. Otherwise, it is the most stable in time with temperature relative maxima of T ~ -1.45 °C and T ~ -1.61 °C at S ~ 30.8 and S ~ 33.3, respectively. A lower halocline is also present.

The Turner angle is plotted verses depth for each of the previous ten-days segments (Figure 15). The data used to calculate the Turner angle and the molecular heat fluxes was low-pass filtered at 0.5 m^{-1}. The gray scale was chosen to maximize features within a given plot and is not consistent between figures. The Turner angle not only divides the water column into the diffusive regimes, but also clearly depicts the layered structure of the different water masses. In the Beaufort Sea, a layer grew where Tu < -45° at 40 m, and a sustained band was present from 45 m to 60 m (Figure 15a). These correspond to the negative temperature gradients toward the temperature maxima at 42m and 62 m. Several bands of Tu<-45° appear for various durations. The longest continuously observed was near 80 m.

In the Northwind Rise region, a layer where Tu ~ -45° was immediately below the mixed layer (Figure 15b). Between 40 m to 60 m was a strongly diffusive region. This corresponded to the intensifying negative, thermal gradient as the BSSW signal became stronger. The distribution of Tu in the Northwind Rise region was very erratic, lacking persistent layers that were present in the other geographic regions. This increasing BSSW signal suggests that this is a region of BSSW inflow and consequently more contrast between different water masses. The vertical interleaving creates strong vertical gradients, and the spatial and temporal variability of Tu suggests this is a region of horizontal mixing.

The Chukchi Plateau Turner angle diagram (Figure 15c) shows the quickly evolving structure that was present in this region's T-S diagram (Figure 14c). Prior to day 98144, many weak bands were present. After day 98144, numerous oscillations around Tu = -45°were present, which correspond to the rapidly changing sign of the thermal gradient. The high variability of Tu after day 98144 suggests a region of vertical interleaving and horizontal mixing, but the lower values of Tu imply that the contrast between the water masses is not as strong as in the Northwind Rise region.

Over the Mendelev Abyssal Plateau, the 5 m immediately below the mixed layer was a region with Tu < -45° (Figure 15d). In this layer, warmer water was insulated from the mixed layer by the pycnocline. Slight stratification was present in most of the upper halocline, but the Turner angle remained nearly constant at approximately Tu ~ –45°. A region favorable for weak diffusive convection was evident below 130 m, where the thermal gradient became more strongly negative.

For each ten-day period, a histogram of the relative frequency of the Turner angle in the vertical water column is shown in Figure 16. The data spans the depth interval from 10 m to 120 m, and the histogram is plotted in 2-degree bins. The Northwind Rise and Chukchi Plateau regions have wider distributions of Tu, while the Mendelev Abyssal Plain distribution is almost entirely in the Tu = -44°-45° bin. A vertical profile with gradual vertical changes in temperature and salinity is expected to have a Tu ~-45, as discussed in section II.C. A wide distribution of Tu is indicative of an interleaved structure, and a larger standard deviation implies larger vertical gradients.

The percent of each profile with Tu less than –50°, where Tu < -50° is indicative of stronger diffusive convection, is shown in Figure 17. The percent of Tu < -50° is greatest in the Northwind Rise region after 98025 with profiles consistently exhibiting convective diffusive capability greater than 20 percent; whereas, the other regions are almost all less than ten percent.

The water masses in the Northwind Rise region and the Chukchi Plateau region have more interleaved structure due to the horizontal inhomogeneity of the water masses. Because the physical processes that influence the halocline have time scales greater than a day, the abrupt transition to highly variable Tu in the Northwind Rise region after day 98024 and in the Chukchi Plateau region after 98144 shown in Figure 15 suggest that these regions contain a vertical structure with horizontal variations (i.e., observed changes are due to variations in space, not variations in time).

The molecular heat flux is plotted verses depth over the ten days in Figure 18. Again, the gray scale was chosen to maximize features within a given plot and is not consistent between figures. In the Beaufort Sea, multiple layers are evident from the

mixed layer to 80 m (Figure 18a). Molecular fluxes into the mixed layer reached 0.08 W/m^2. A layer at 50 m is present for the 10-day sample with positive fluxes ranging from 0.01 to 0.04 W/m^2.

In the Northwind Rise region, there was positive flux into the mixed layer up to 0.05 W/m^2 (Figure 18b). Regions of rapid fluctuations appeared as the warmer BSW was sampled. The strongest molecular flux of the entire data set (0.2 W/m^2) was on day 98027 of with a duration of half a day.

The Chukchi Plateau region is shown in Figure 18c. Prior to day 98144, many layers of sustained fluxes evolved, with the strongest at approximately 35 m with a positive flux of 0.07 W/m^2. After day 144, many fluctuations in the layered structure occurred.

Figure 18d shows sustained positive molecular fluxes of 0.02 W/m^2 into the mixed layer. This low positive flux was the result of the relative T_{max} ~-1.4 °C at 30 m. Sustained positive flux of 0.01 W/m^2 was present coming from warm layer below 130 m, indicative of the lower halocline above the Atlantic layer.

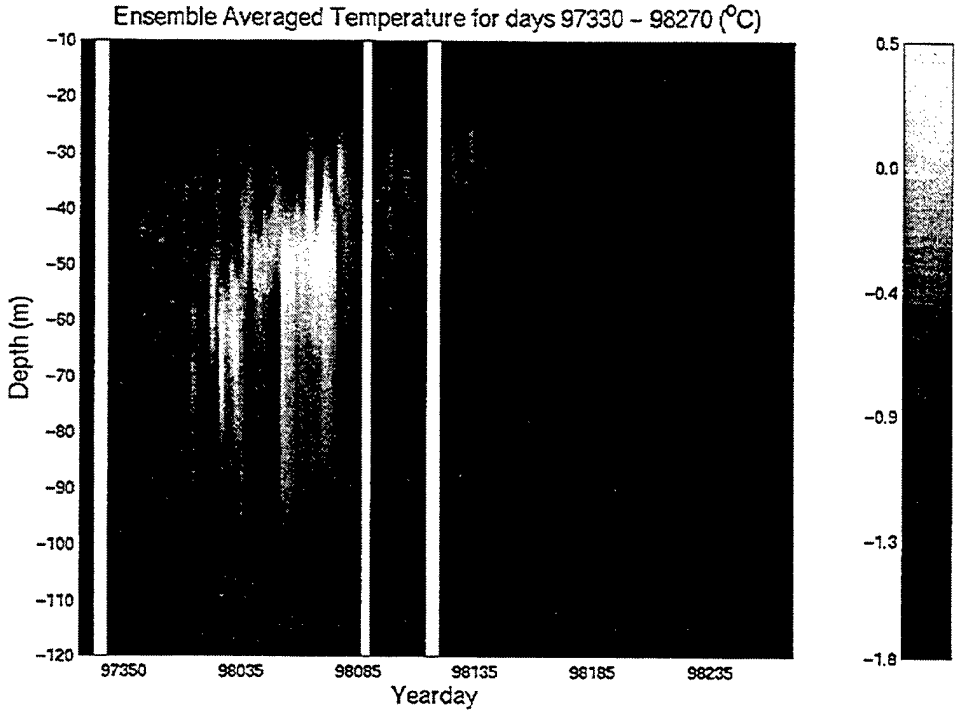

Figure 5. The 1-day ensemble averaged temperature for the entire data set.

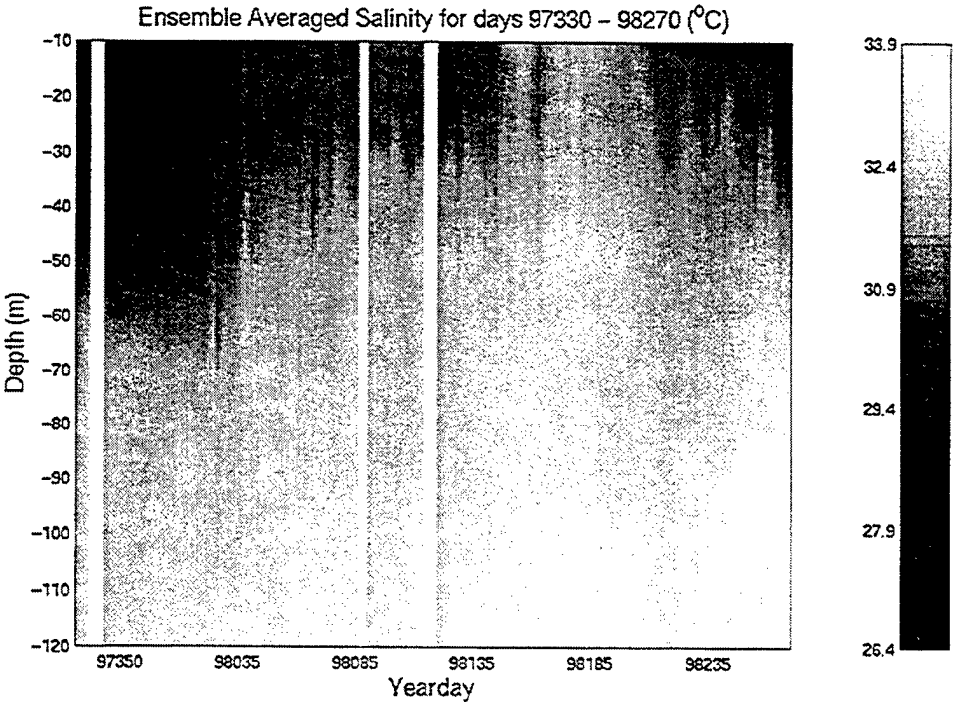

Figure 6. The 1-day ensemble averaged salinity for the entire data set.

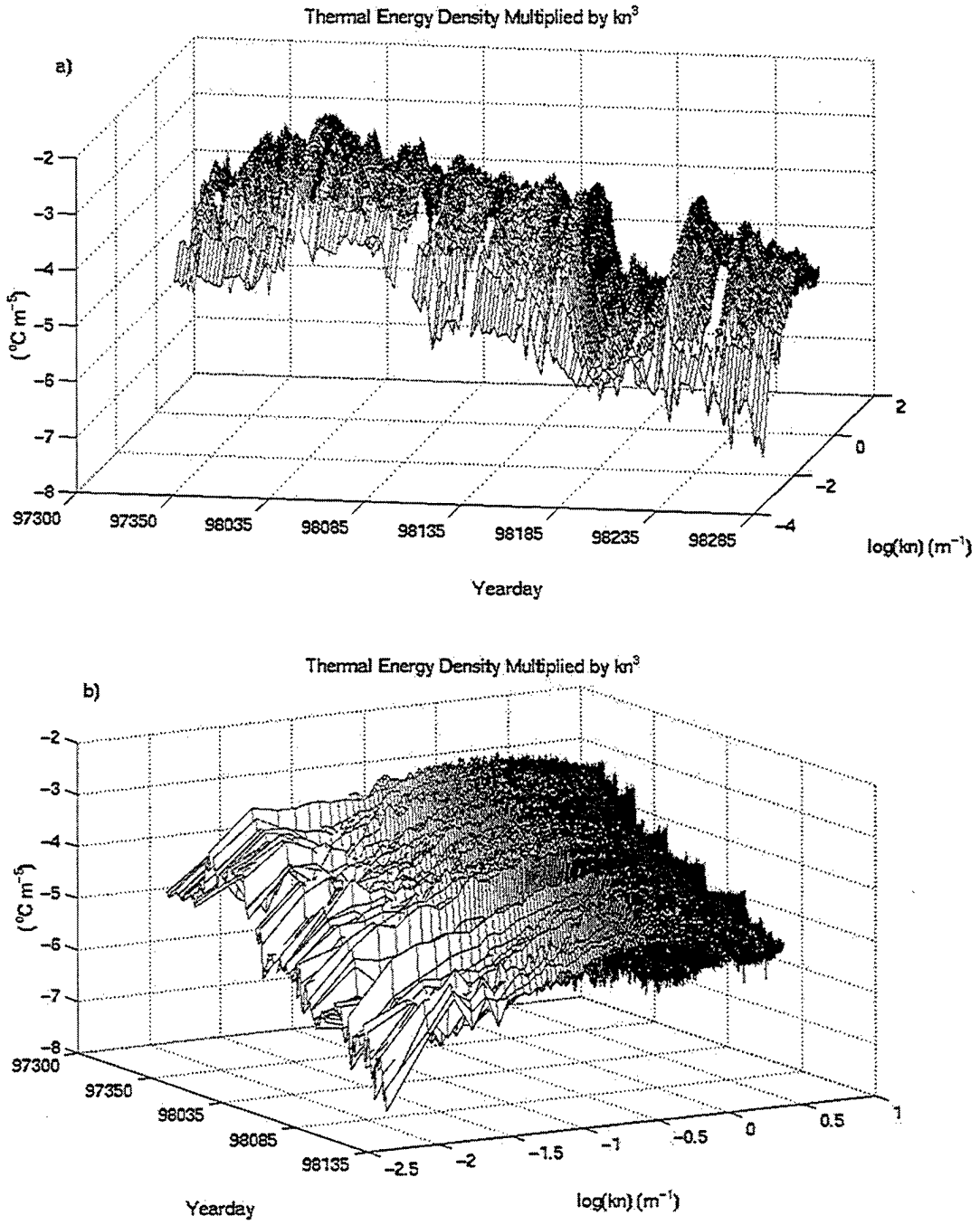

Figure 7. a) The evolution of the thermal spectra multiplied by the wavenumber cubed over the entire data set. b) Same as a), but viewed from an angle to emphasize the shape of the spectra. Note the vertical axes are 10^{-2}, 10^{-3}, etc.

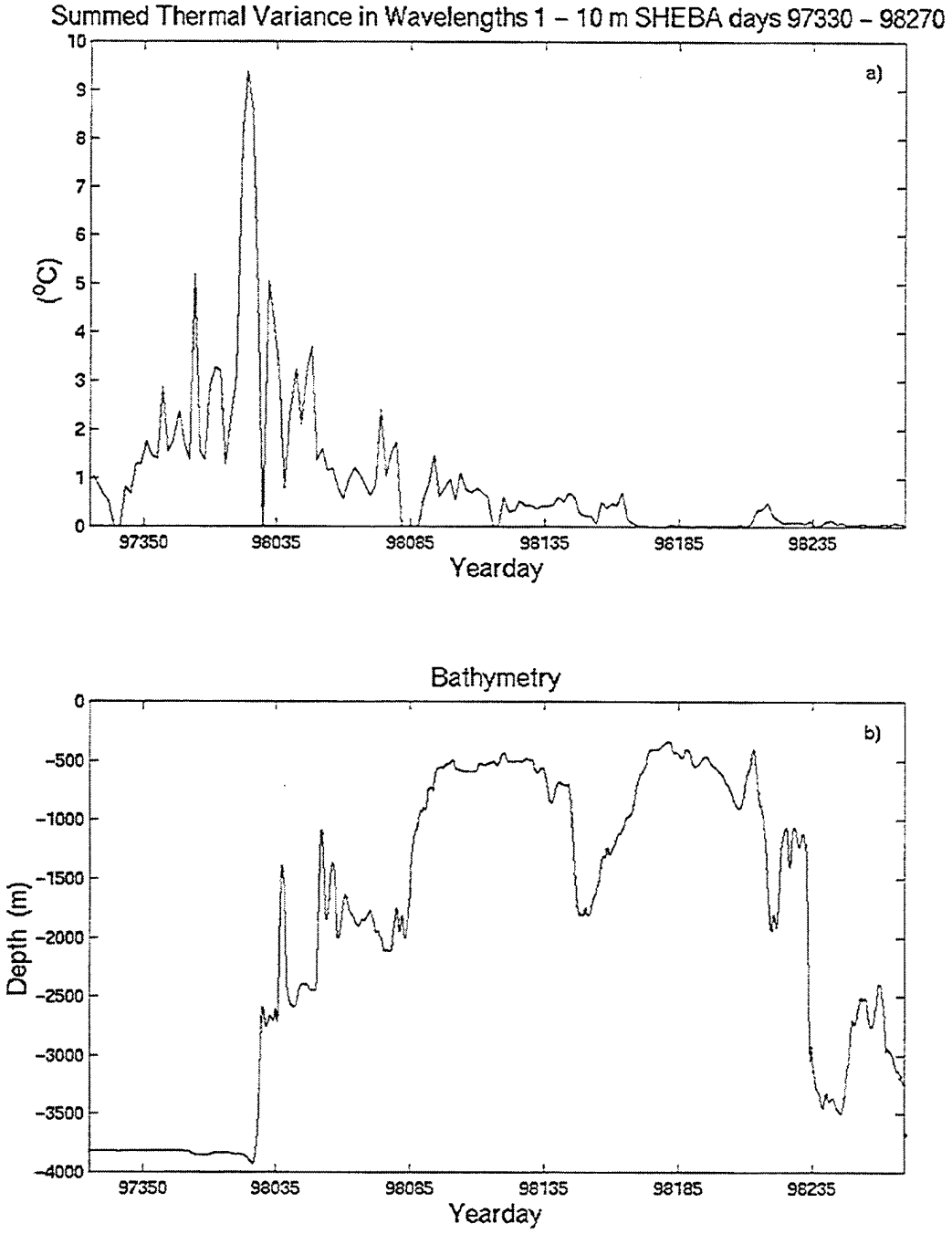

Figure 8. a) Thermal variance with wavelengths between 1 m – 10 m summed over the entire data set. b) The bathymetry beneath the SHEBA ice station track for the entire data set.

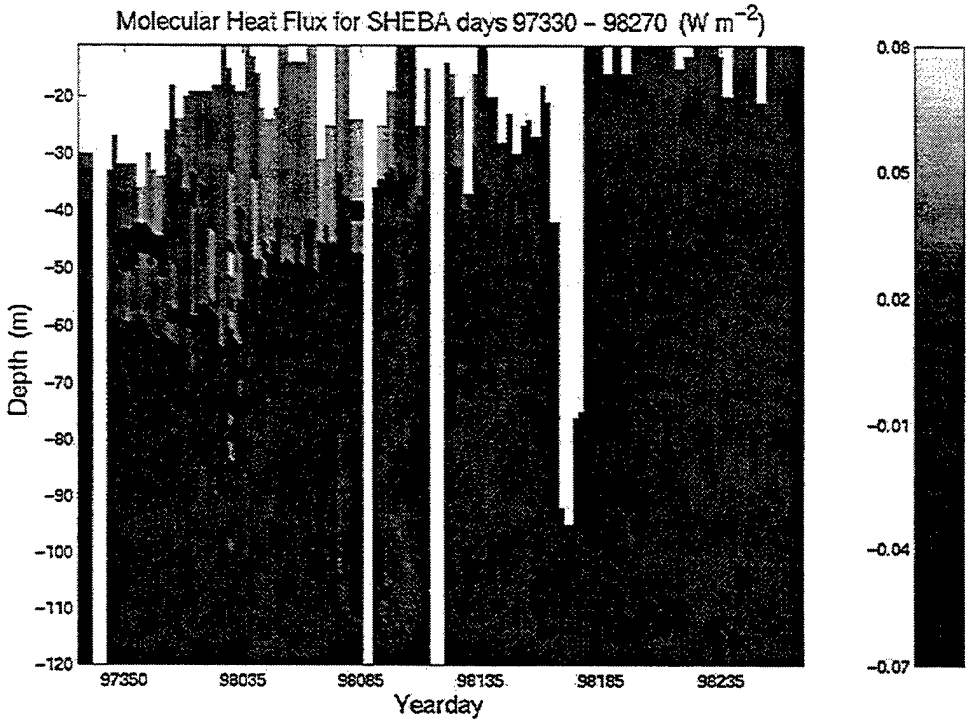

Figure 9. The 1-day ensemble averaged molecular heat flux for the entire data set.

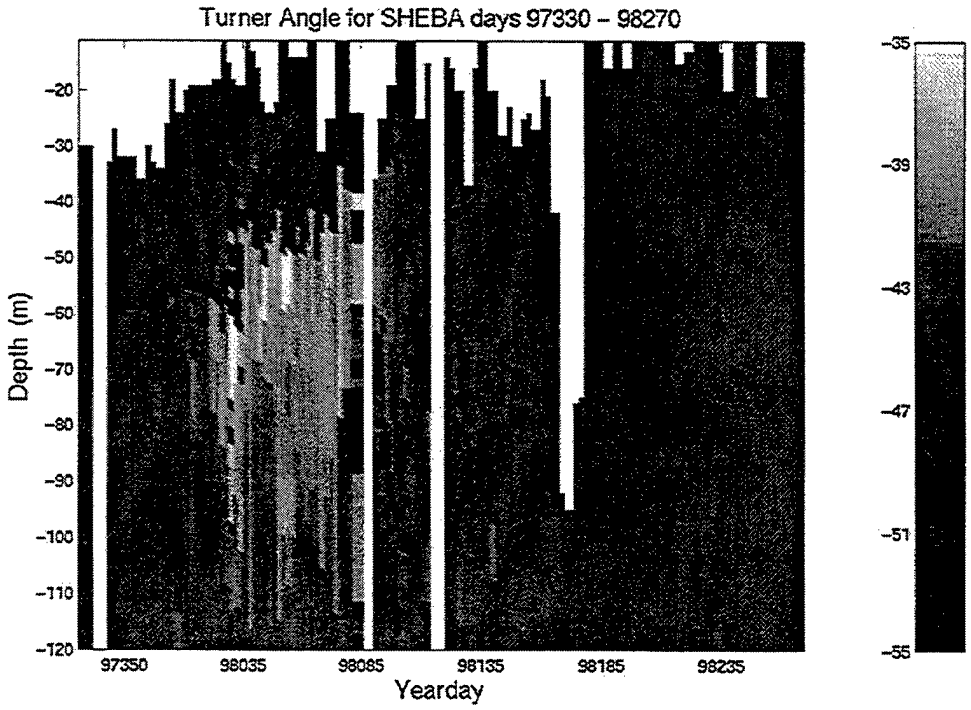

Figure 10. The 1-day ensemble averaged Turner angle for the entire data set.

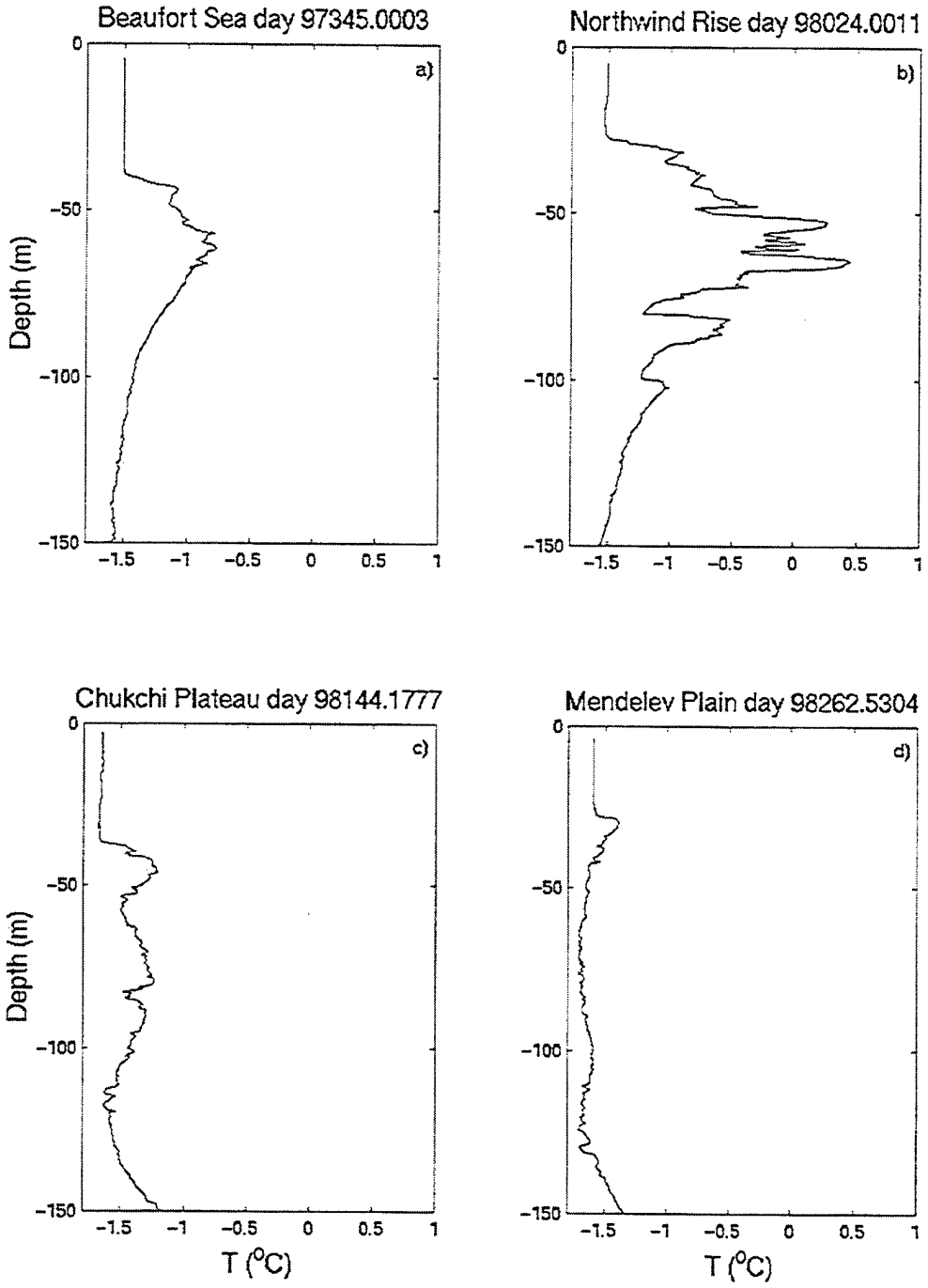

Figure 11. Vertical temperature profiles representative of the four regions. a) Beaufort Sea. b) Northwind Rise. c) Chukchi Plateau. d) Mendelev Abyssal Plain.

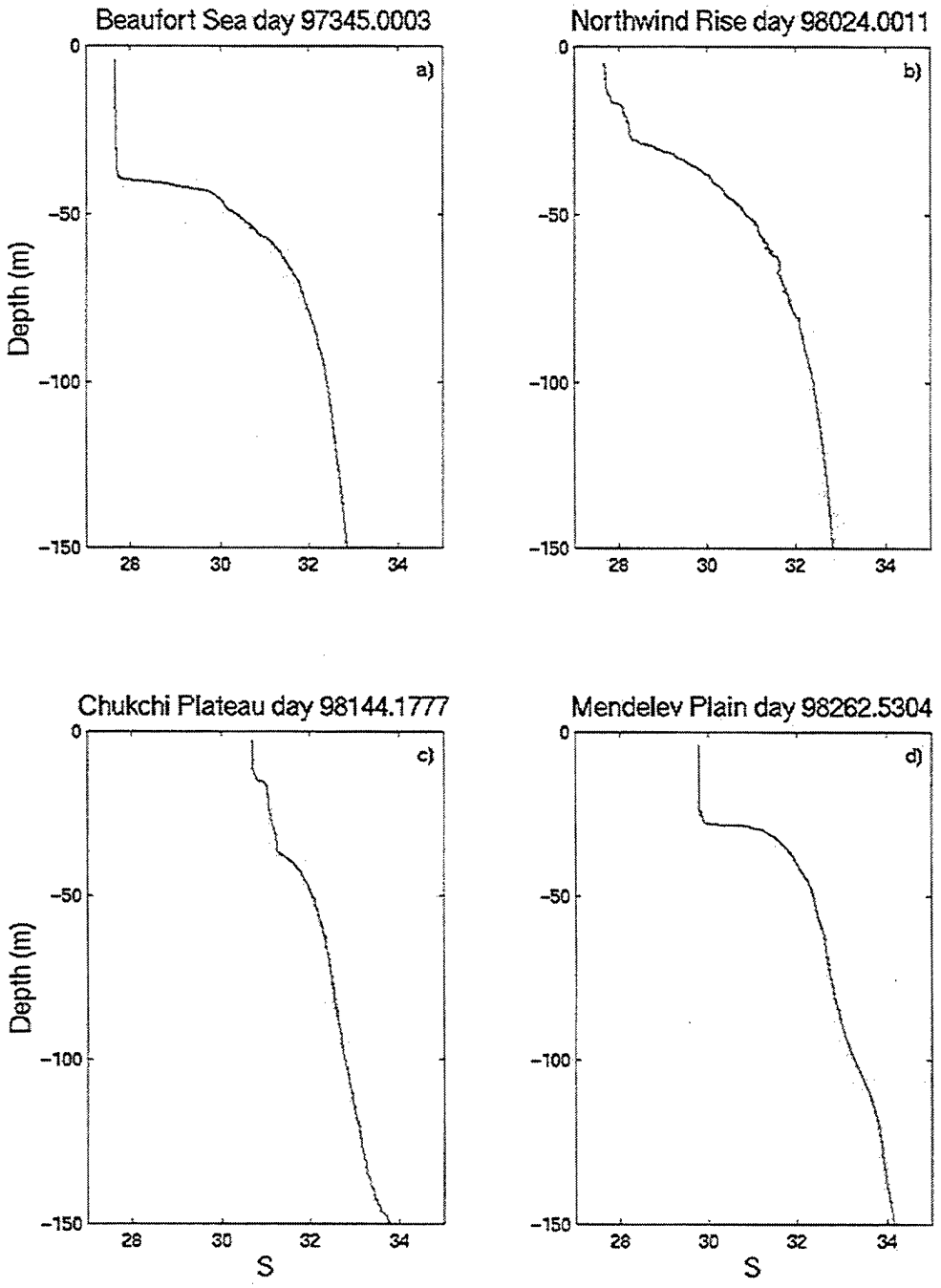

Figure 12. Vertical salinity profiles representative of the four regions. a) Beaufort Sea. b) Northwind Rise. c) Chukchi Plateau. d) Mendelev Abyssal Plain.

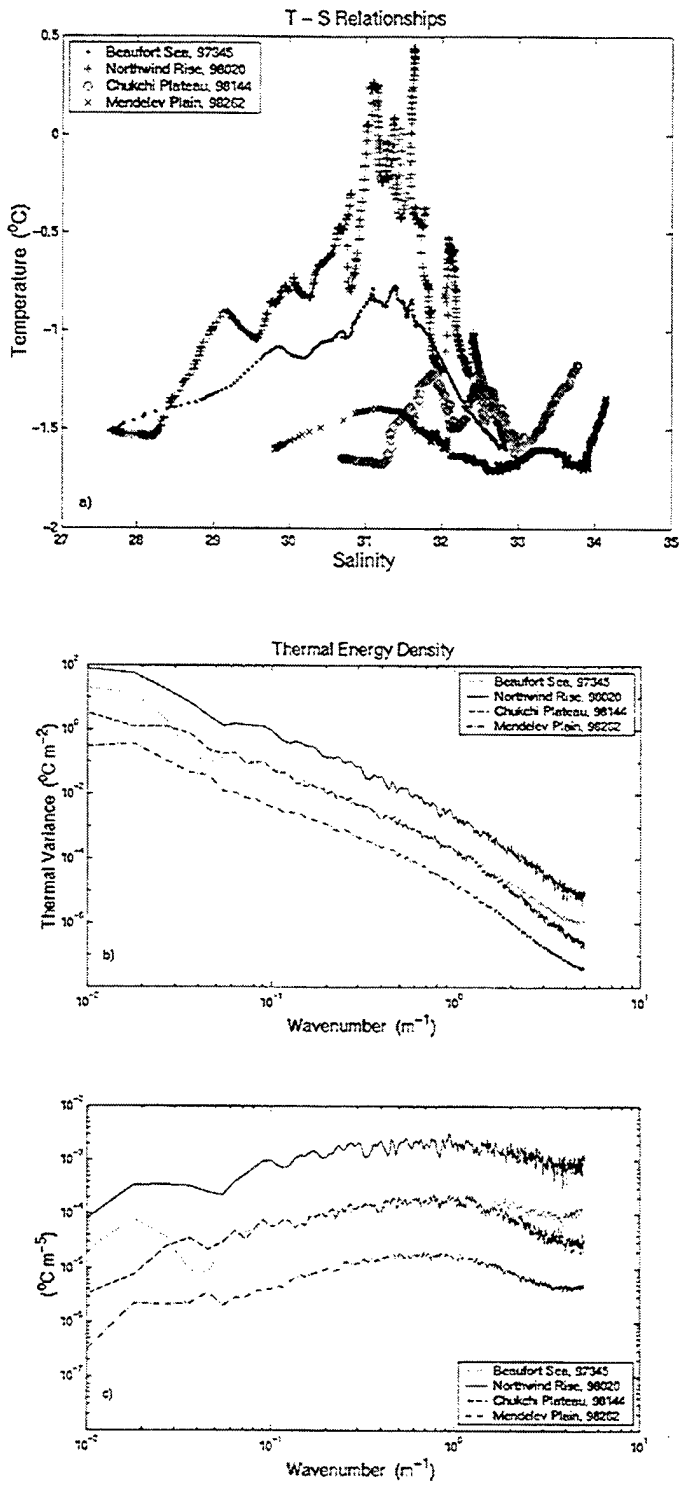

Figure 13. a) Overlaid T-S plots. b) Overlaid thermal spectra. c) Overlaid thermal spectra multiplied by the wavenumber cubed.

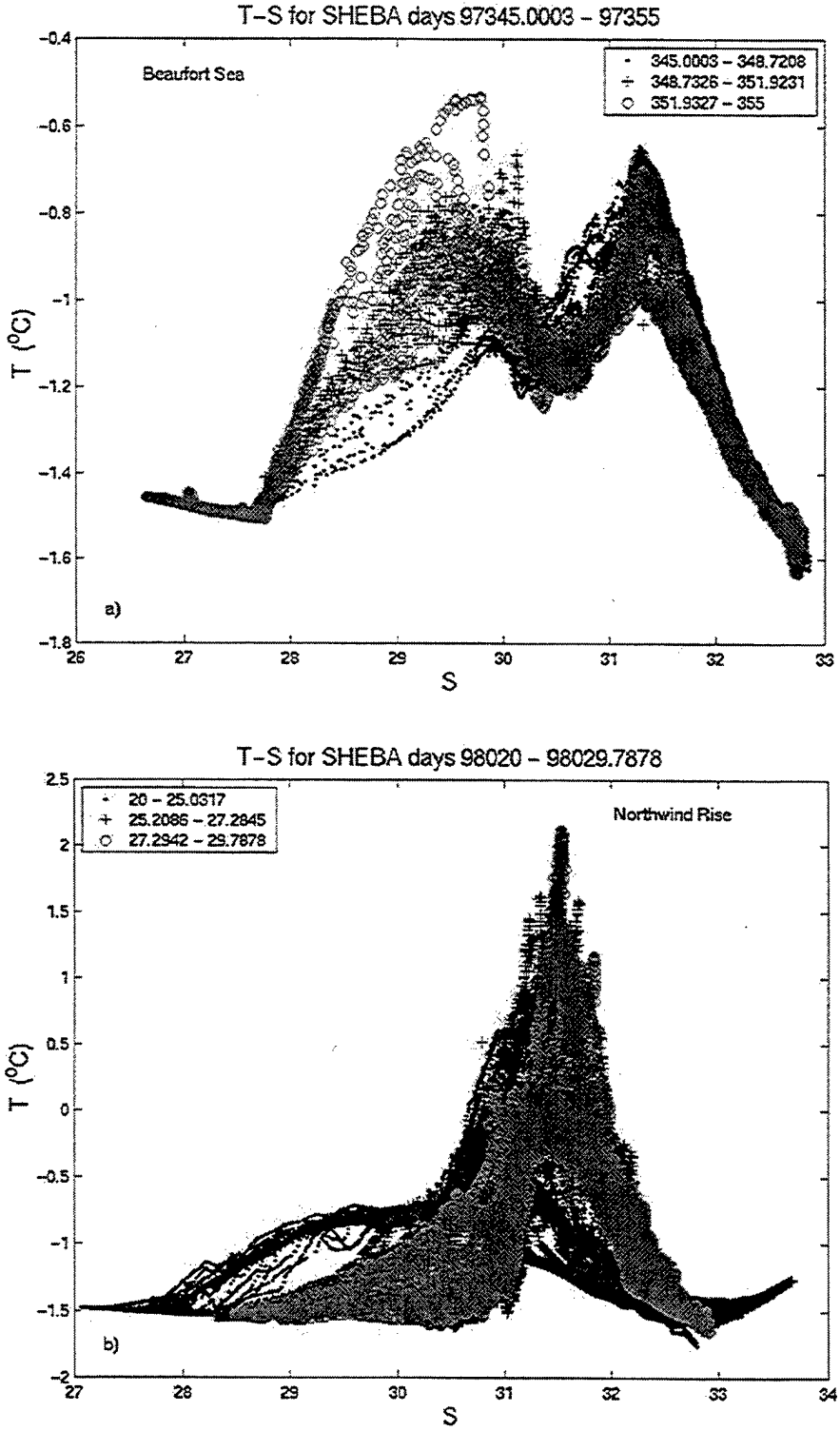

Figure 14. The evolution of T-S Profiles. a) Beaufort Sea region. b) Northwind Rise region. c) Chukchi Plateau region. d) Mendelev Abyssal Plain region. Note the T and S scales differ for each region.

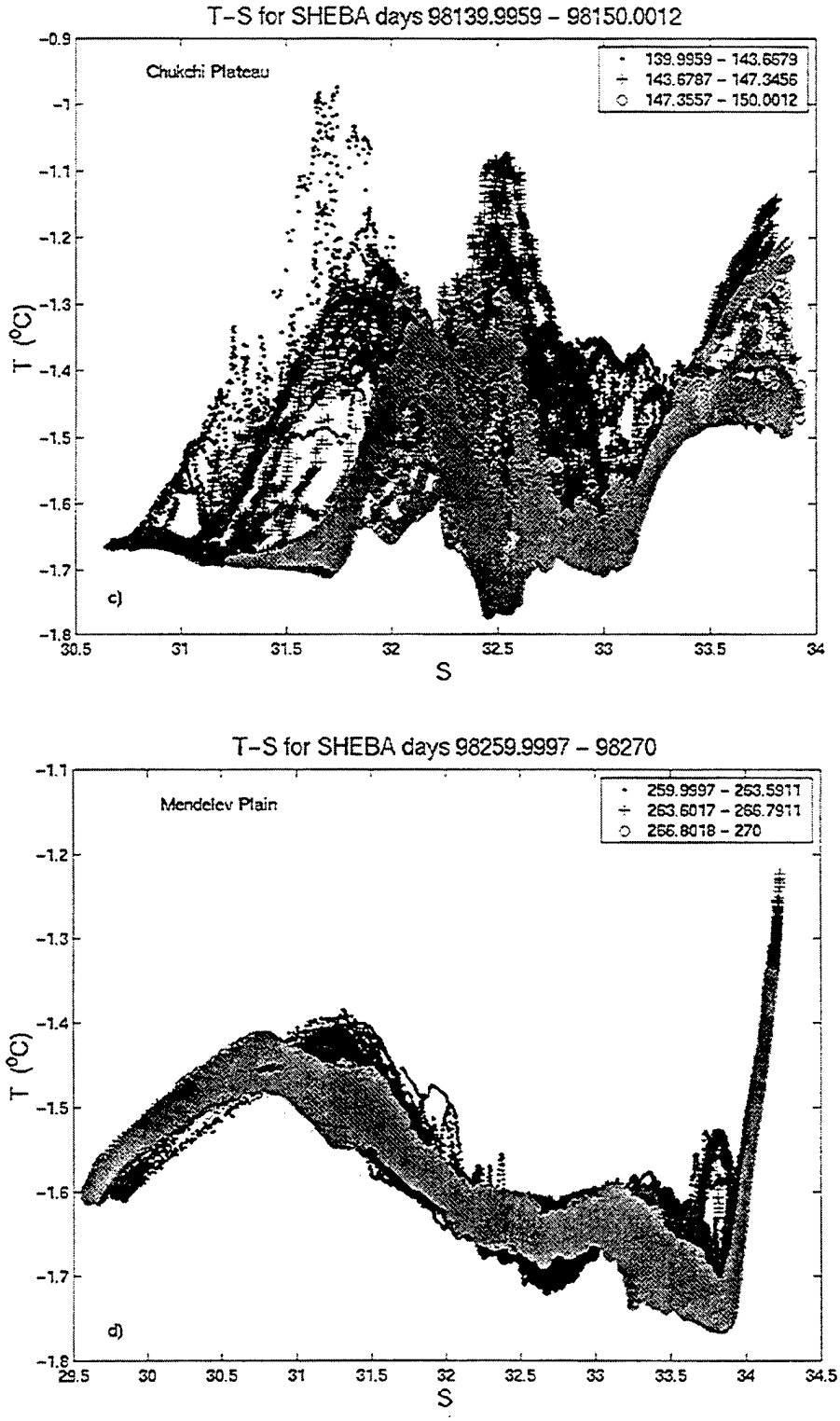

Figure 14. c) Chukchi Plateau region. d) Mendelev Abyssal Plain region.

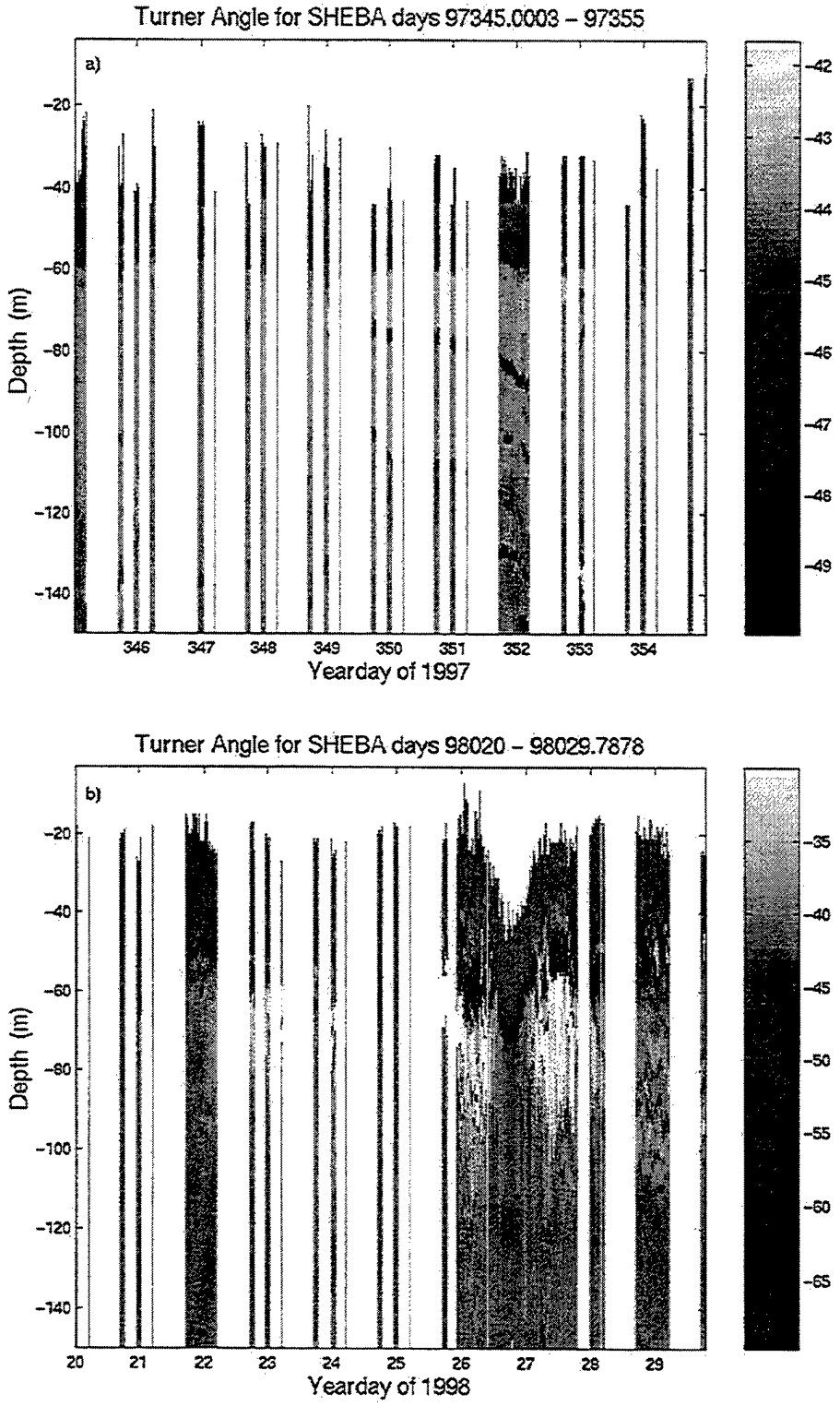

Figure 15. Turner angle over ten day periods. a) Beaufort Sea region. b) Northwind Rise region. c) Chukchi Plateau region. d) Mendelev Abyssal Plain region. Note the Turner angle gray scales differ for each region.

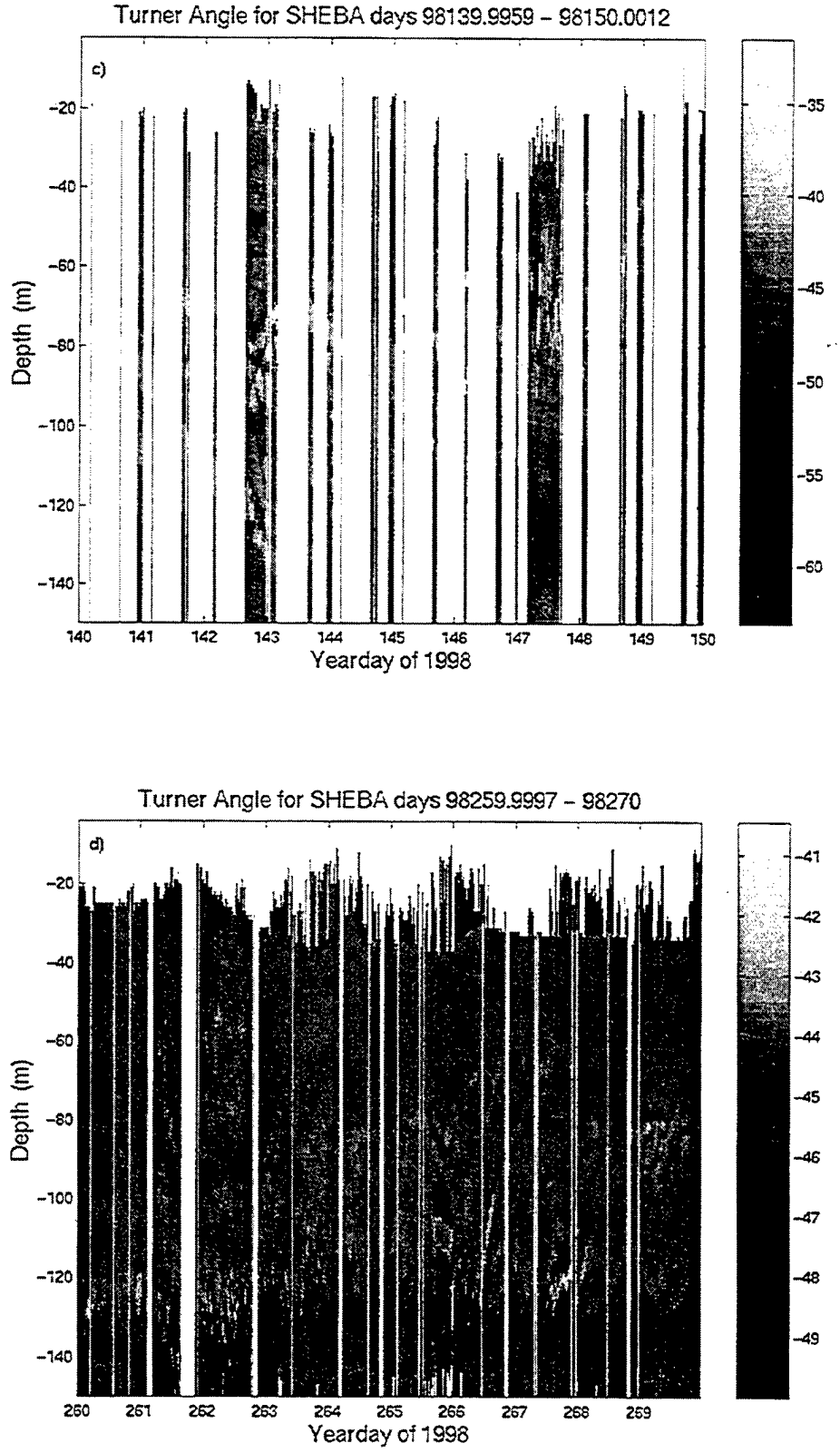

Figure 15. c) Chukchi Plateau region. d) Mendelev Abyssal Plain region.TU c,d

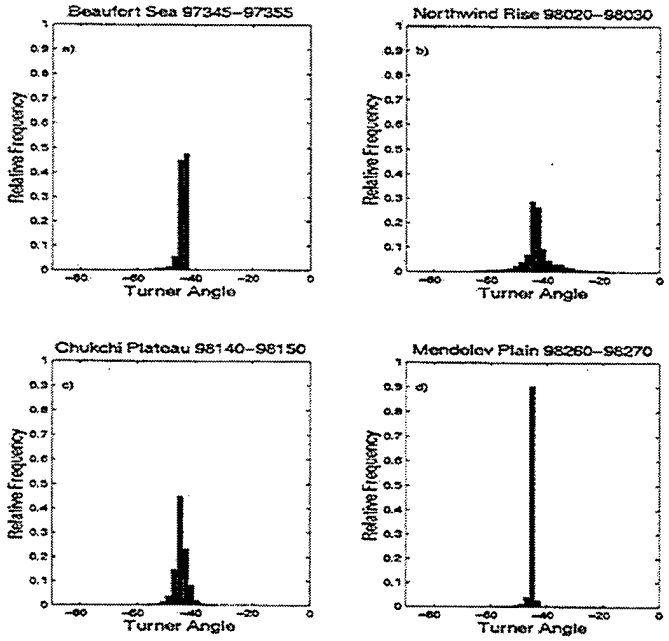

Figure 16. Histogram of Turner angles over ten day periods. a) Beaufort Sea region. b) Northwind Rise region. c) Chukchi Plateau region. d) Mendelev Abyssal Plain region.

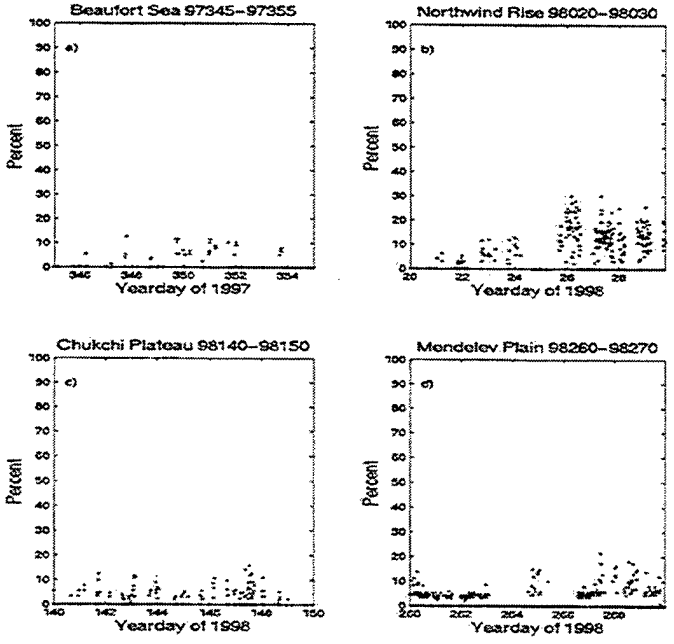

Figure 17. The percent of each vertical profile with Tu < -50° over ten days. a) Beaufort Sea region. b) Northwind Rise region. c) Chukchi Plateau region. d) Mendelev Abyssal Plain region.

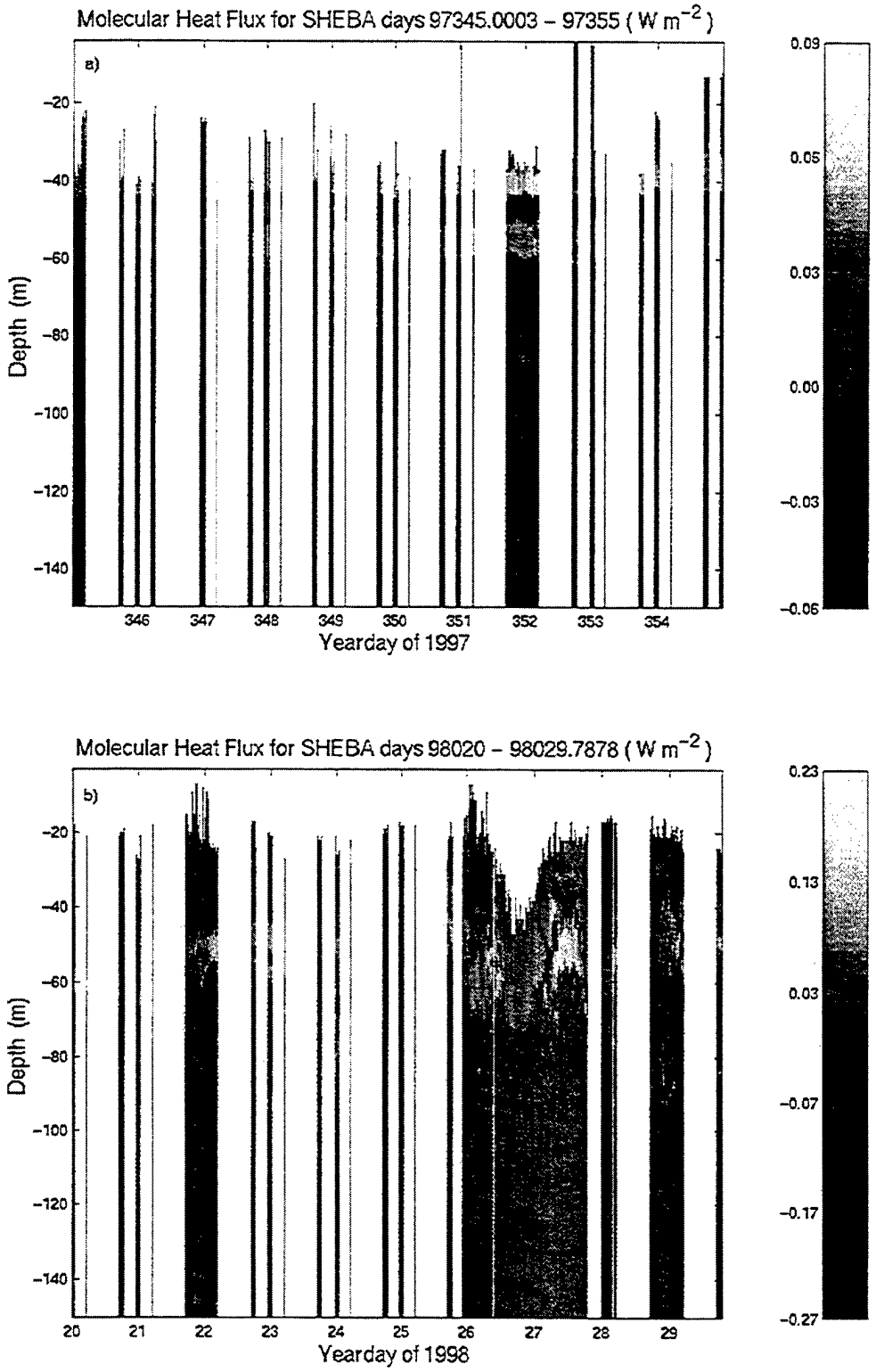

Figure 18. Molecular heat flux over ten day periods. a) Beaufort Sea region. b) Northwind Rise region. c) Chukchi Plateau region. d) Mendelev Abyssal Plain region. Note the molecular heat flux gray scales differ for each region.

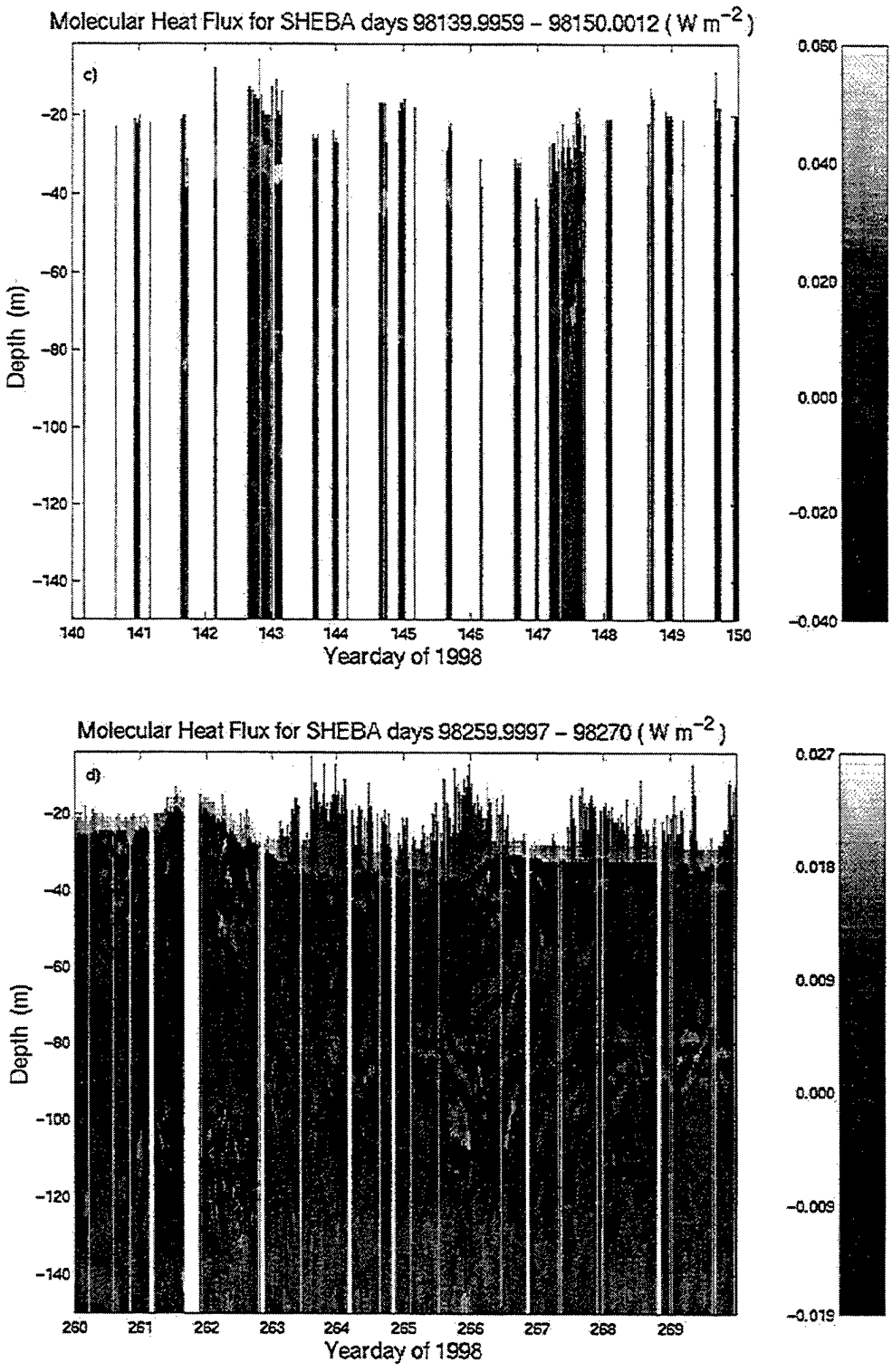

Figure 18. c) Chukchi Plateau region. d) Mendelev Abyssal Plain region.

THIS PAGE INTENTIONALLY LEFT BLANK

V. DISCUSSION

A. THE REGIONAL EXTENT OF BSSW

The eastern branch of the Bering Sea inflow enters the Beaufort Sea through Barrow Canyon. The T_{max} signal for BSSW became strong in the Northwind Rise region because the SHEBA ice camp drifted into the BSSW inflow region and associated eddy field. The ice camp was 170 km west of the submesoscale coherent vortices (SCVs) sampled during AIWEX *(D'Asaro*, 1988a). As the BSSW flows through Barrow Canyon, frictional torque along the canyon wall reduces the potential vorticity of the flow. When the flow exits the canyon, adjustment to conserve potential vorticity generates anticyclonic SCVs (*D'Asaro*, 1988b). SCVs have been found to be most common in the core of the warm water intrusion of BSSW into the Beaufort Sea. The vortices then propagate into the central Beaufort Sea carrying BSSW in their cores.

The average flow through Barrow Canyon is along the canyon axis, but episodic reversals occur and water from the intermediate layer flows up the canyon (Weingartner et al., 1998). Thus inflow into the Beaufort Sea has interruptions as opposed to a steady flow conceptualization. Furthermore, although the BSSW inflow is concentrated through Barrow Canyon, lesser amounts flow directly over the Chukchi Shelf into the Canadian Basin (Coachman et al., 1975). Consequently, lateral inhomogeneities will be present between different intrusions.

From yearday 98026.3 – 98027.2, the ice station drifted over a SCV (Figure 19a). Because of the along track nature of the CTD sampling and the inability to make regional surveys, the full extent of the SCV could not be ascertained. During this time, the ice

camp followed a curved track across the eddy spanning 23 km. This represents a lower bound on the diameter of the eddy. The SCV's sampled in AIWEX had diameters of 10 – 20 km. The dominant feature of the SCV is the double domed geometry of the contoured isopycnals, which reveals anticyclonic flow, maintaining the gradient balance. Enhanced internal wave activity was associated with the eddy, seen in the oscillations in the isopycnals and by the elevated levels of the one-hour to ten-minute band passed standard deviation of the depth of the 25.75 isopycnal (Figure 20).

Eddies and SCVs are efficient mechanisms for the transport of water mass properties and energy over large distances (*Gill*, 1982). Lateral intrusions in eddies have been shown to mix heat, salt, and angular momentum radially outward (*Ruddick*, 1992). A feedback loop exists where the vertically sheared lateral advection produces double diffusive lateral gradients. The double diffusive fluxes and associated buoyancy flux convergence, as described in section II.C, produce density perturbations, which cause pressure gradients that reinforce the original lateral advection (*Ruddick*, 1992). Furthermore, the large velocity shear in azmuthal velocity and internal waves act as a kinetic energy source for small-scale turbulent mixing. As viscous dissipation removes the kinetic energy, double diffusive fluxes are established that further reduce temperature and salinity gradients at longer timescales (*Williams*, 1981).

Vertical profiles from inside and outside the eddy encountered on day 98026 are shown in Figure 21. The main BSSW inflow, which spanned a depth of approximately 50 m, is fragmented into smaller intrusions with vertical extents on the order of 5 m. The coupled shear/double diffusive process is hypothesized to be the mechanism responsible for the increased interleaving of the smaller layers present in the main BSSW inflow.

When the SCV has decayed or in regions where there are no SCVs, the intrusion process works in a similar manner. The velocity shear is less due to the absence of azimuthal velocity, but internal waves and the shear as the intrusion slides between the upper and lower layers can still be a source of kinetic energy.

In a conceptualization of BSSW inflow into the Beaufort Sea and Northwind Rise regions, the Bering Sea inflow and associated eddy field penetrate into the Beaufort Sea with the T_{max} of the BSSW intruding on the 25.8 isopycnal. Variations in volume transport into the Beaufort Sea create horizontal variations in the distribution of the BSSW temperature signal. The SCVs represent an anomalous kinetic energy source in the quiescent basin interior that fragments the BSSW inflow into smaller lateral intrusions that spread out at their respective densities. The vertical interleaving erodes the structure of both the BSSW and associated SCVs, resulting in a laterally well-mixed region with persistent layers of BSSW located at the top of the upper halocline. The more recent BSSW inflows possess stronger gradients in the interleaving, with wider distribution of Turner angles, and a greater portion of the water column possessing Turner angle values less than -45°. Therefore, the Northwind Rise region contained the relatively most recent BSSW, and the Mendelev region contained the oldest.

Visualization of this process is supported by model output from the Polar Ice Prediction 3.0 (PIPS 3.0) model currently under development (*Maslowski*, 2000). The model spin-up is forced by 15-year atmospheric data derived from the European Center for Medium Range Weather Forecasting (ECMWF) 1979-1983 data. Once spin-up is complete, model runs are forced by 1979-1998 daily atmospheric data in an attempt to better simulate seasonal variability. The model domain includes the Arctic Ocean, the

North Pacific, and the North Atlantic. Figure 22 shows the average velocity at depths from 99 m to 268 m from the model. The coordinate axes represent a portion of the model domain. Between Barrow Canyon and the Chukchi Plateau, eddy-like features are persistently seen in the simulation.

A BSSW temperature signal (T_{max} at ~75 m with 31<S<32) was present from yearday 97330 until approximately 98144, as the ice station drifted from the Beaufort Sea to the Northwind Rise and over a portion of the Chukchi Shelf. The T_{max} ~ 2 °C at 60m found in the Northwind Rise region was 2.3 °C warmer than the T_{max} in the Beaufort Sea. The relative T_{max} ~ -0.7 °C was intermittently present as the ice station grazed the Chukchi Shelf, where the bottom depth was 500 m. The BSSW abruptly disappeared on day 98144 as the ice camp drifted over the Chukchi Shelf break and the water depth briefly increased to 1700 m. A weaker BSSW temperature signal with T_{max} ~ -1.2 °C returned as ice camp drifted over the Chukchi Plateau, and the depth progressively decreased to 500 m. After the ice station drifted off the plateau and into the Mendelev Abyssal Plain region, the BSSW signal was concentrated in a narrow layer approximately 5 – 10 m thick, immediately below the mixed layer and at the top of the upper halocline. The T_{max} in the Mendelev region was approximately –1.4 °C.

The western branch of Bering Sea inflow enters the Canada Basin through Herald Canyon. Although the Mendelev Abyssal Plain lies at the head of Herald Canyon, only a weak BSSW signal was found in the region. The BSSW was concentrated in a narrow layer immediately below the mixed layer. During the period of the SHEBA drift, the frontal boundary that separates the eastern Arctic waters with Atlantic characteristics from the western Arctic waters of Pacific origin was located between the Mendelev

Ridge and Chukchi Plateau and extended to the Chukchi Shelf (*Morison et al.*, 1998). A proposed synoptic circulation increased the eastern Arctic flow from the East Siberian Sea into the Canada Basin (*Tyner*, 1997). This may have reduced the amount of BSSW flow through Herald Canyon, accounting for the absence of a strong BSSW signal in the Mendelev Abyssal plain region.

B. COLD INTRUSIONS

During yearday 98044-98049, the water depth along the drift track abruptly increased from 600 m to 1700 m in the Chukchi Plateau region as the ice camp drifted across a shelf break front (Figure 23). This was also a region of increased internal wave activity and strong interleaving (Figure 20c). The sloping isopycnals induced geostrophic flow. As with eddies, the kinetic energy present in the geostrophic flow and the velocity shear induced by internal wave activity is coupled to the double diffusive process as described previously with the result being increased lateral and vertical mixing. The highly variable interleaved structure evident in Figure 15c from days 98144 - 98150 is indicative of this process.

The Chukchi Plateau region has the closest geographic proximity to the Chukchi Shelf. Cold intrusions in this region are expected due to the shelf drainage processes described in section II.A. The freezing point departure is the difference between the temperature of a water parcel at a given salinity and the freezing point at that salinity. Because the generation of cold intrusions on the continental shelf requires the water to be at the freezing temperature, cold intrusions can be identified where the freezing point departure is less than 0.1 °C. Cold intrusions were encountered only after the ice camp

crossed the shelf break front on yearday 98148, and then were predominately situated over the Chukchi Plateau as shown in Figure 24. Figure 25 shows cold intrusions with the T-S properties of $T < -1.7$ °C and $32.5 < S < 32.8$ at $\sigma_t \sim 26.2$. Waters with these properties have been observed in previous studies. The USGC *Polar Star* made a transect heading off the Chukchi Shelf approximately 500 km to the southeast in August 1993 (*Weingartner*, 1998). The transect revealed a plume with similar properties ($T < -1.7$ °C and $32.5 < S < 32.9$) that spanned a depth from 50 m to 120 m.

The ice camp drift carried it closest to the Chukchi Shelf on yeardays 98085 – 98140. Several questions arise: if the source of the cold intrusions is the Chukchi Shelf, why do the cold intrusions appear immediately after the ice camp drifted across the shelf break front into deeper water? Why are the intrusions confined to the Chukchi Plateau? The ice camp was over the Chukchi Plateau in July and August. It is possible that the intrusions were formed on the shelf in winter and propagated to the Chukchi Plateau by July. If the intrusions are topographically constrained by the topography to conserve potential vorticity $q = (f + \zeta) /H$, as an intrusion enters deeper water, it would either propagate north or establish a clockwise rotation. Neither of these responses was observed due to the slow drift rate through the Chukchi Plateau region, which precluded synoptic measurements, and the lack of the ability to conduct regional surveys. More data is required in order to explain the preponderance of cold intrusions over the shallow topography of the Chukchi Plateau.

C. THE ROLE OF INTRUSIONS IN HEAT TRANSPORT

The vertical molecular heat fluxes along the SHEBA drift track were $O(10^{-2})$ W m^{-2}. Theoretically, formulations for the effective molecular diffusivity show that under optimum conditions for diffusive convection, the molecular diffusivity will be increased by a factor of three (i.e., $K_{eff}=3K \sim 4.2 \times 10\text{-}7\ m^2s^{-1}$) (*Kelley*, 1984). The maximum molecular heat flux value for this study, ~0.2 Wm^{-2} and corresponding Tu ~ -65°, were obtained while sampling the SCV in the Northwind Rise region. The small diffusivity coefficients enable this heat to remain confined to the intrusions until more energetic processes mix the BSSW to other layers. An intrusion which penetrates the basin interior at an isopycnal deep enough to avoid entrainment into the mixed layer may traverse a significant distance from its origin. Therefore, intrusions have the potential to transport water mass properties throughout the Canadian Basin as they slowly decay. This was seen with the nearly ubiquitous BSSW salinity signal that possessed a temperature that decreased with distance from Barrow Canyon.

As the BSSW intrusions slowly move into the basin interior, they carry heat isolated from the mixed layer by the pycnocline. The available heat (H_a, Wm^{-2}) in the vertical column is defined below:

$$H_a = \int \rho c_p \left(T(z) - T_f(s)\right) dz \qquad \text{Eq. 2}$$

where $T(z) - T_f(s)$ is the freezing point departure (i.e., the difference between the temperature as a function of depth and the freezing temperature as a function of salinity). Figure 26a shows the one-day ensemble averaged vertical temperature profiles from yeardays 97355 and 98070 from the Beaufort Sea and Northwind Rise regions, respectively. The Northwind Rise profile represents the maximum vertical extent of the

BSSW thermal signal. Figure 26b contrasts the available heat in selected vertical profiles. The two profiles from the Northwind Rise region show the evolution of the available heat as the BSSW layer thickened to span depths from 25 m to 90 m.

The available heat above 40 m in the Northwind Rise region is two orders of magnitude greater than other regions. This represents a reservoir of heat available for entrainment into the mixed layer. If this heat were transferred into the mixed layer with no losses (i.e., the area under the Northwind Rise curve to 40 m in Figure 26), the temperature in an isothermal mixed layer would increase by 0.46 °C. In this context, BSSW intrusions represent a mechanism for the transport of heat from the Bering Sea, through the upper halocline, into the mixed layer of the Canadian Basin.

The available heat below 40 m in the Northwind Rise region was seven orders of magnitude greater than in the Beaufort Sea and eight orders of magnitude greater than the Chukchi Plateau region. The Mendelev Plain region (not shown) was nine orders of magnitude less than the Northwind Rise region. The low diffusivity coefficient and the corresponding low values of molecular heat flux enable the heat intrusions to remain for long periods of time and laterally transport heat into the Canadian Basin interior.

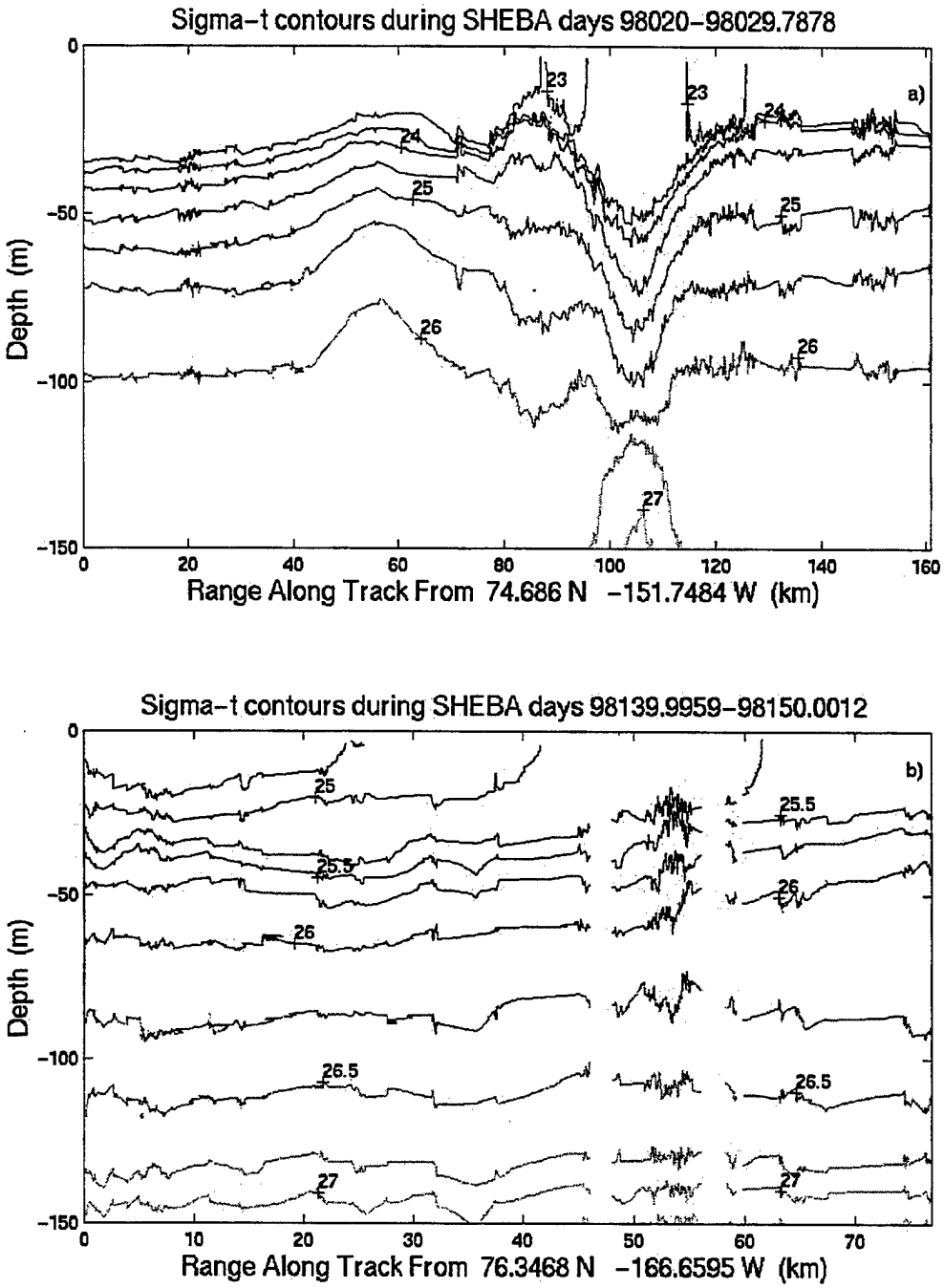

Figure 19. a) Contours of σ_t in Northwind Rise region plotted with respect to distance traveled since yearday 98020.0. b) Contours of σ_t in Chukchi Plateau region plotted with respect to distance traveled since yearday 98140.0.

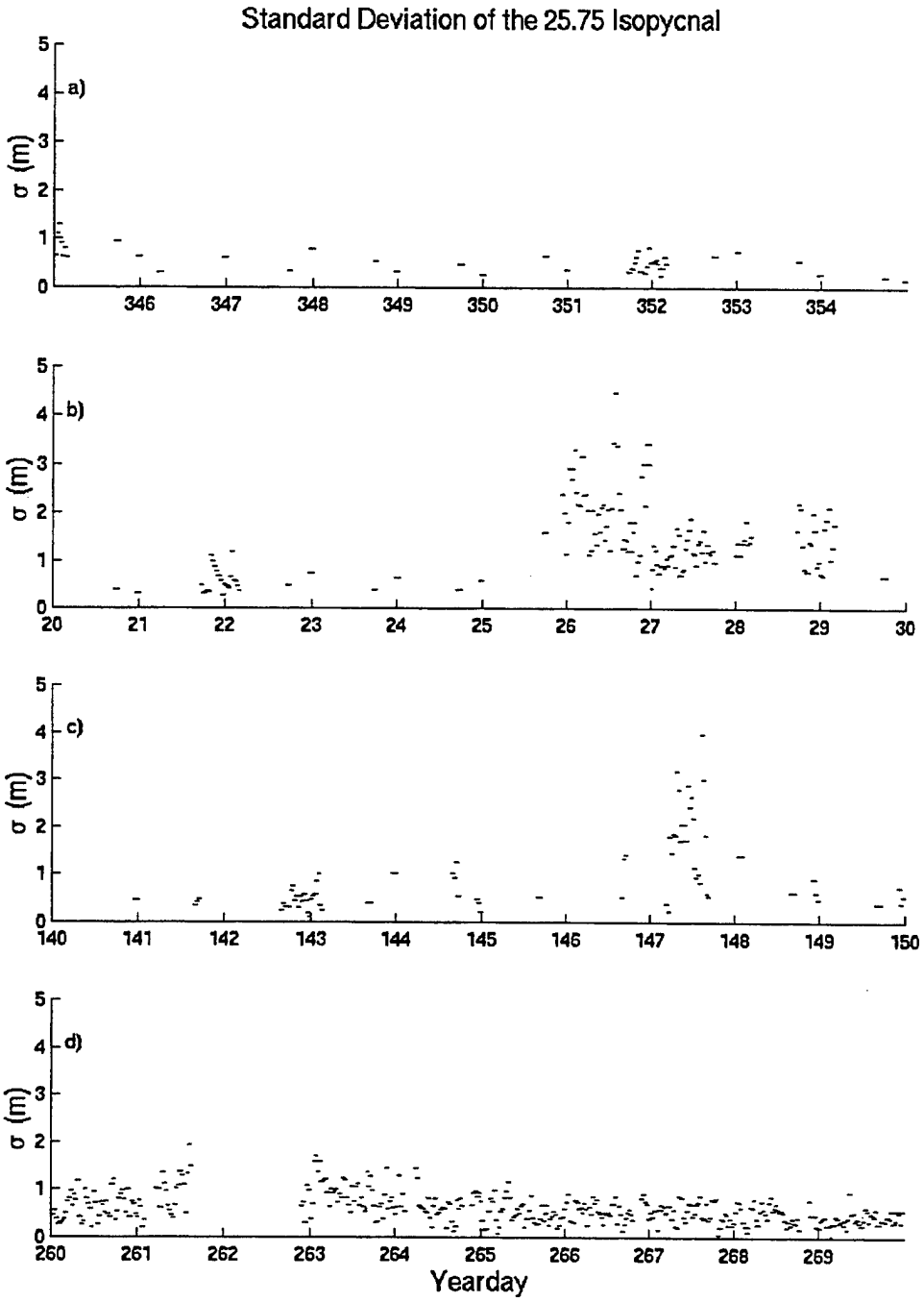

Figure 20. The standard deviation of the depth of the 25.75 isopycnal band passed from one hour to ten minutes. a) Beaufort Sea region. b) Northwind Rise region. c) Chukchi Plateau region. d) Mendelev Abyssal Plain region.

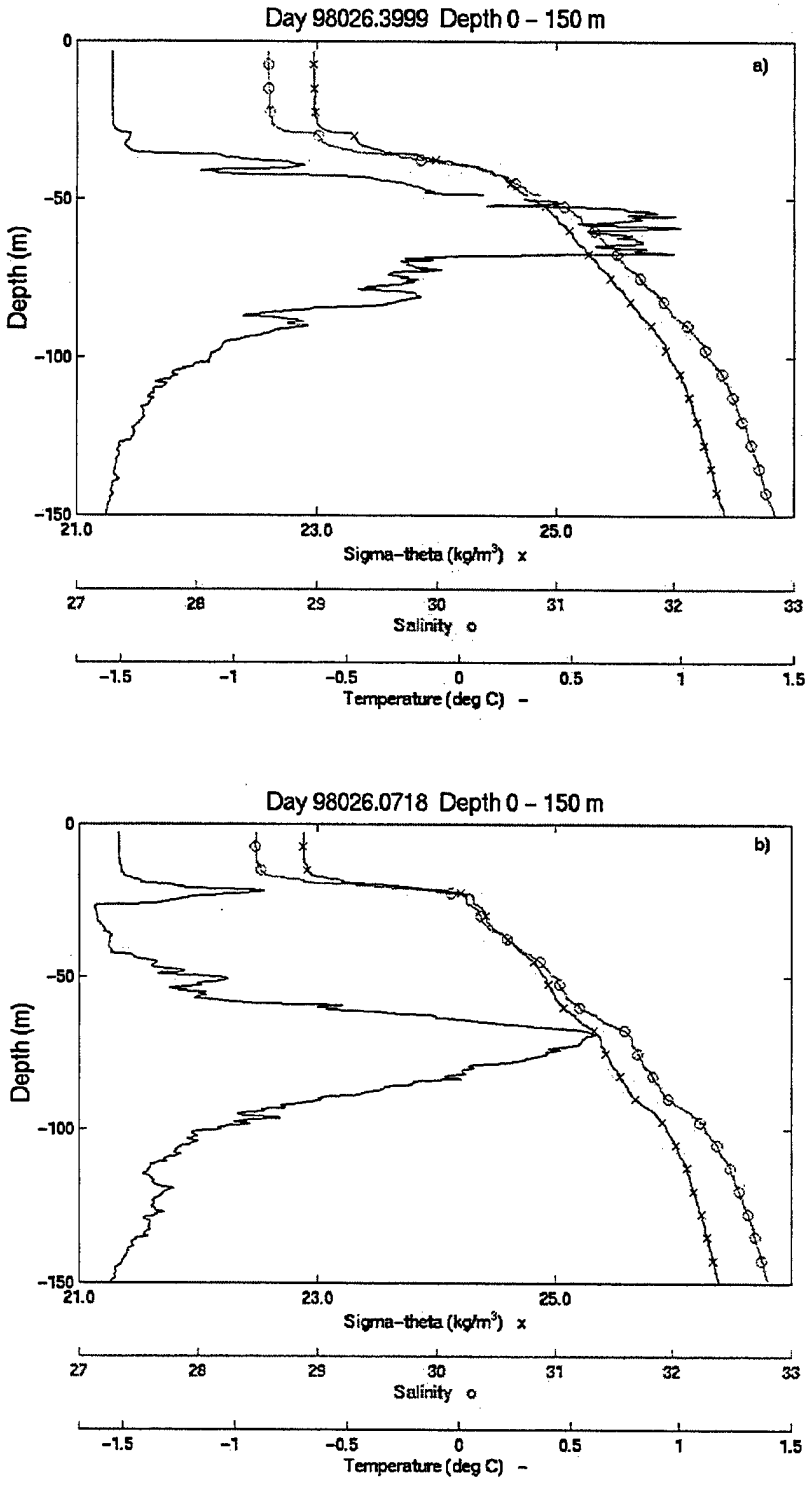

Figure 21. Vertical profiles of temperature, salinity and σ_t. a) Profile inside eddy on day 98026.4. b) Profile outside eddy on day 98026.1.

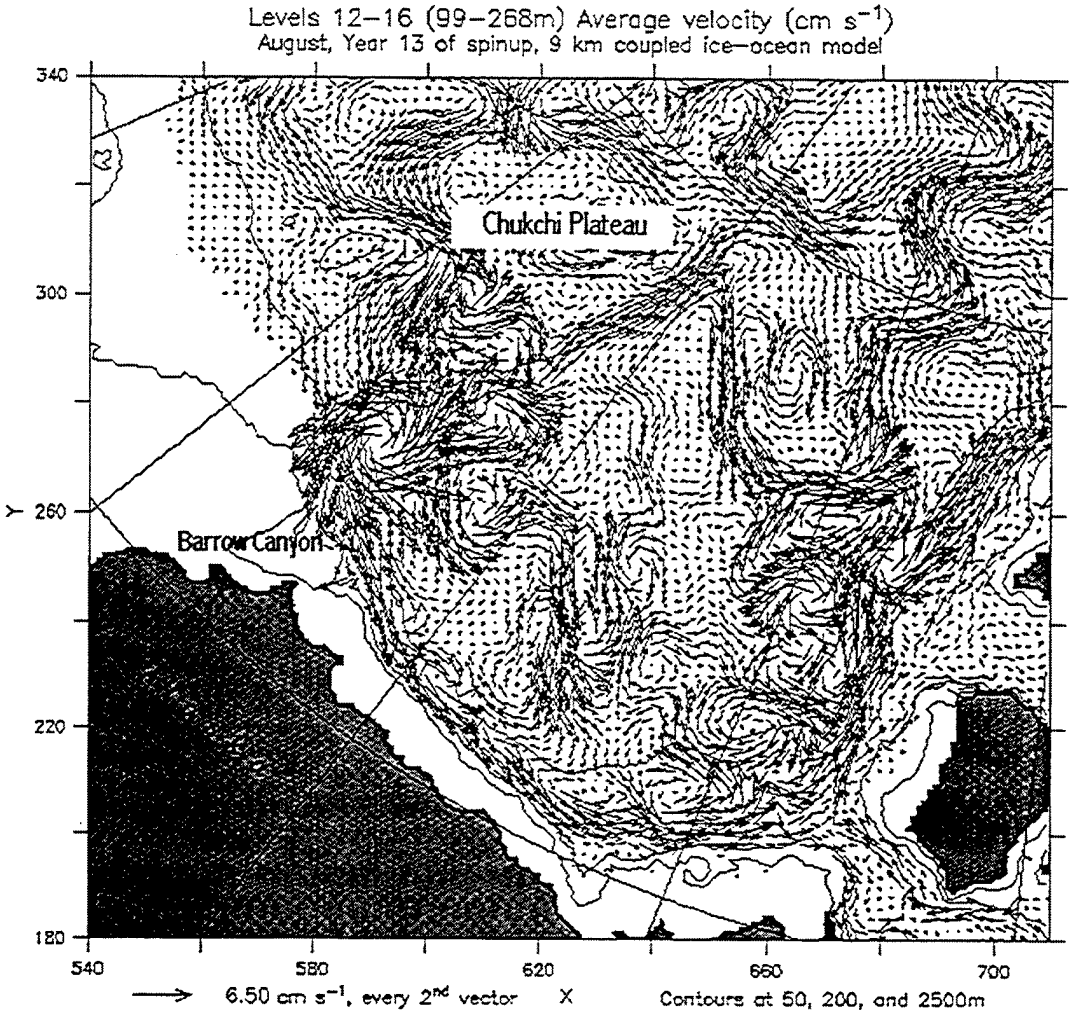

Figure 22. Model simulation of average velocity of depths between 99 m and 268 m. Axes represent a portion of model domain (After *Maslowski*, 2000).

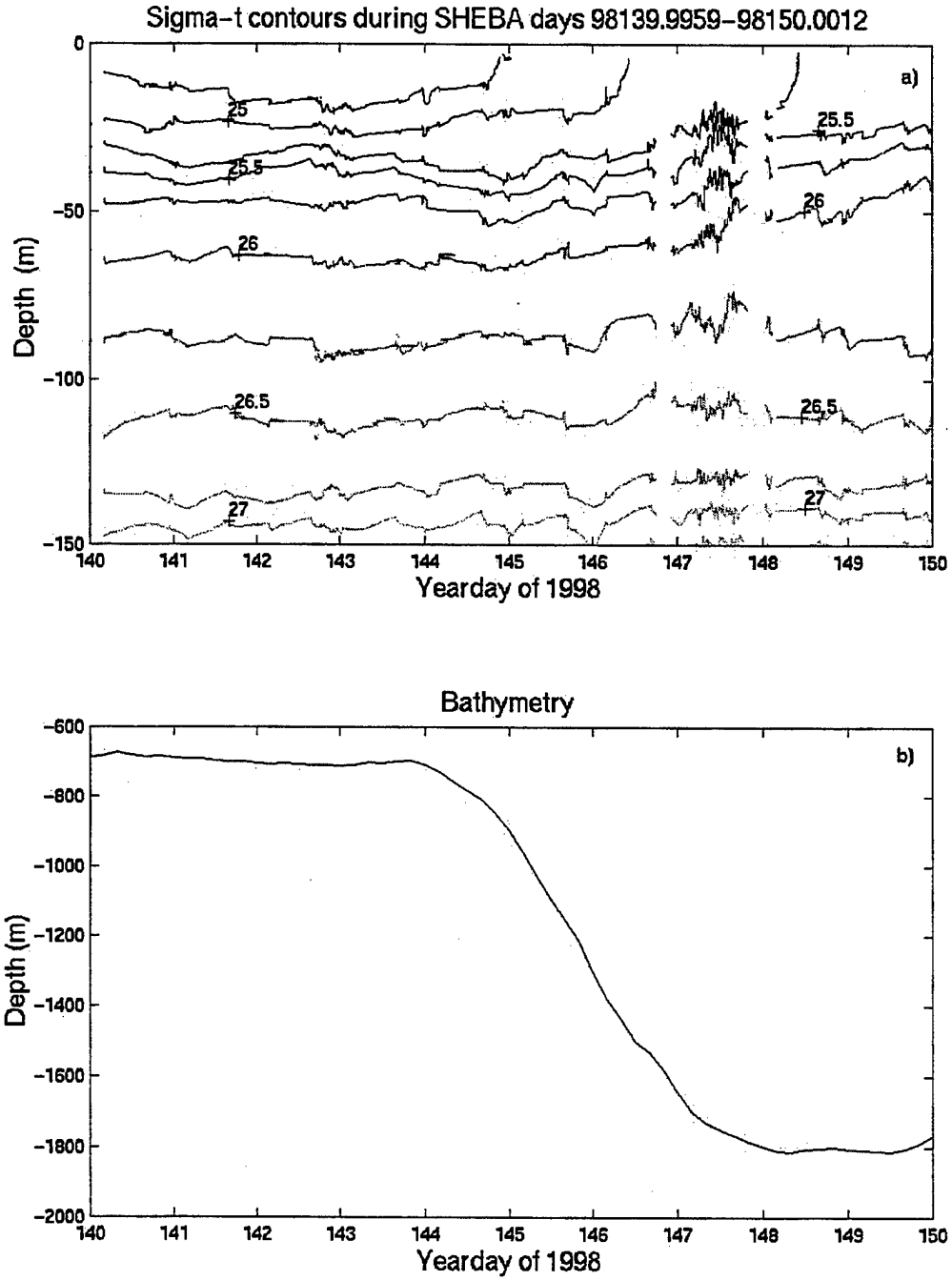

Figure 23. a) Contours of σ_t in Chukchi Platea region during yeardays 98140 – 98150. b) Bathymetry beneath the SHEBA ice station track during the same time period as a).

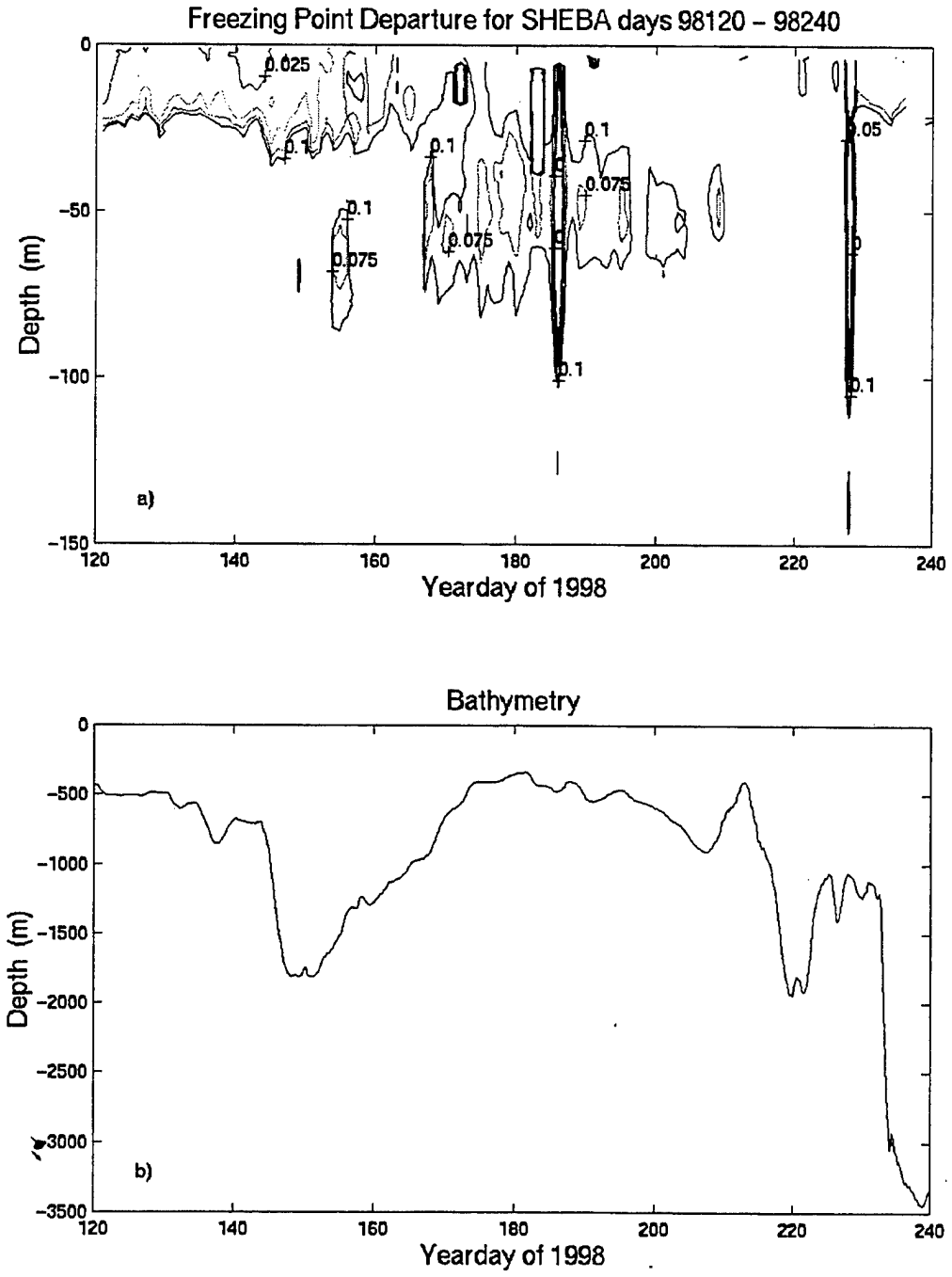

Figure 24. a) Freezing point departure as the SHEBA ice station drifted over the Chukchi Plateau. b) Bathymetry as the SHEBA ice station drifted over the Chukchi Plateau. Contours greater than 0.1 °C were omitted for clarity.

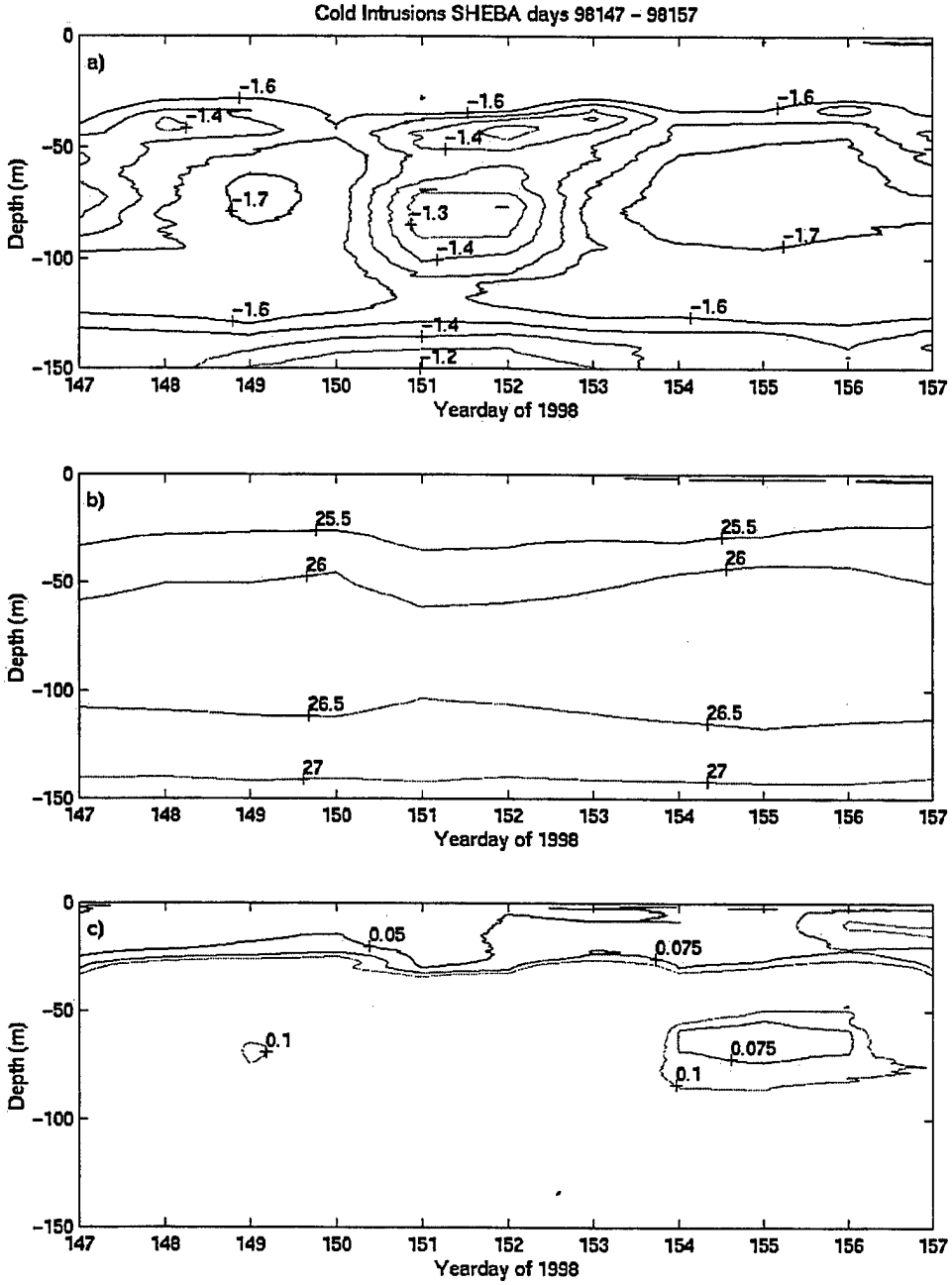

Figure 25. a) Temperature contours during cold intrusions over the Chukchi Plateau during days 98147 - 98157. b) σ_t contours over same time period as a). c) Freezing point departure over same time period as a). Contours greater than 0.1 °C were omitted for clarity.

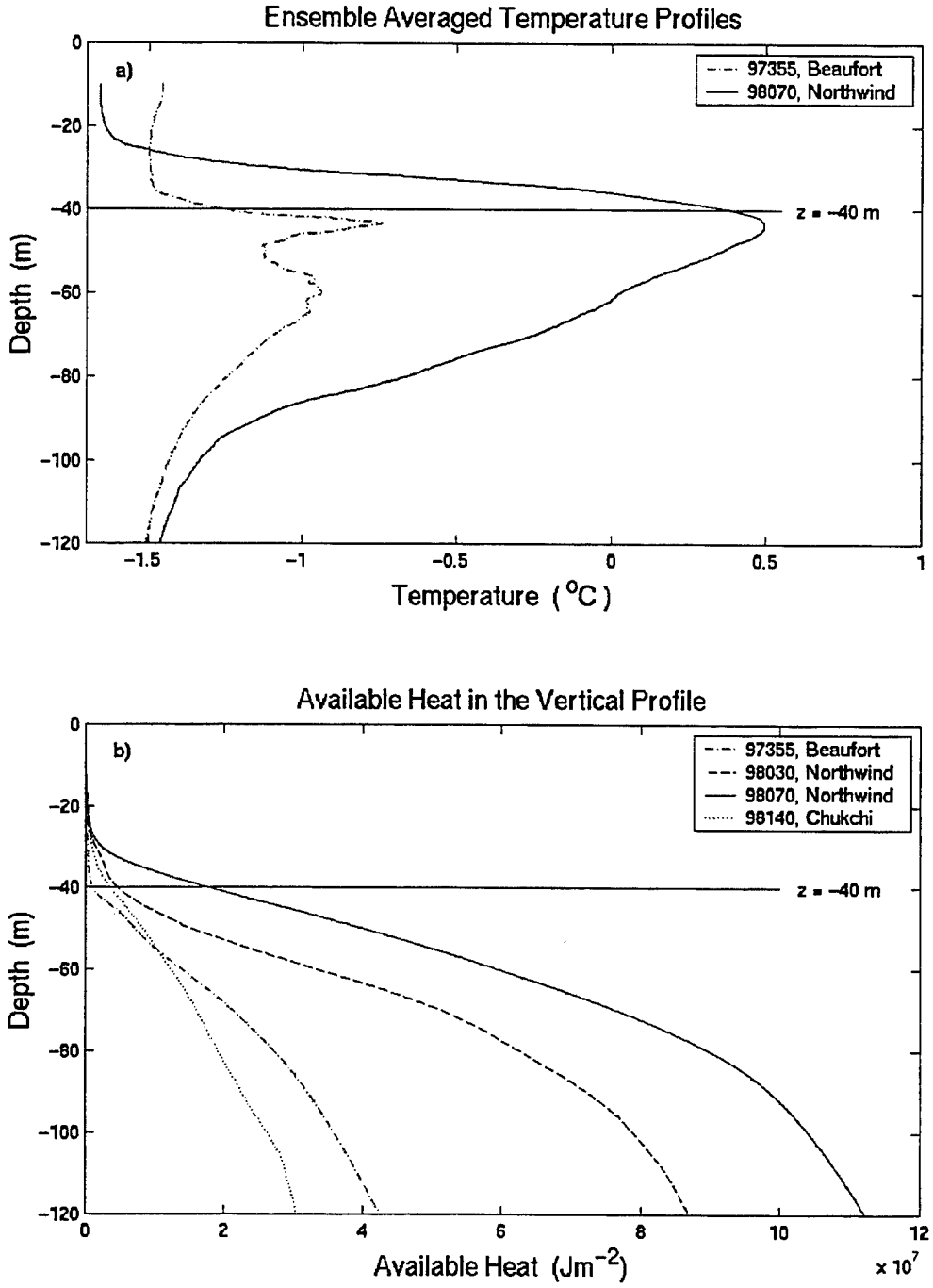

Figure 26. a) One day ensemble averaged vertical temperature profiles for the Beaufort Sea region and, yeardays 97355 and 98070, respectively. b) The available heat in the vertical profile for the same days as a) and additional profiles from the Northwind Rise and Chukchi Plateau regions for comparison.

VI. CONCLUSION

A yearlong set of temperature and salinity profiles from the Surface Heat Budget of the Arctic (SHEBA) experiment were analyzed to identify intrusions from the mixed layer to a depth of 150 m. Ensemble averaged temperature and salinity profiles, spectral analysis of vertical thermal structure, and bathymetry are used to divide the SHEBA ice station track into four regions: Beaufort Sea; Northwind Rise and break; Chukchi Plateau and break; Mendelev Abyssal Plain.

The waters of the basin interior, as characterized by the Beaufort Sea region and the Mendelev Abyssal Plain region, possessed a vertical structure without significant temporal or spatial variability. Bering Sea Summer Water (BSSW) in the Northwind Rise region was repeatedly observed with a maximum temperature greater than 2 °C, which was more than 2.3 °C warmer than the maximum temperature of BSSW observed in the other regions. Mesoscale structures were identified in the Northwind Rise and Chukchi Plateau regions, accompanied with increased internal wave activity. The Turner angle distribution for all regions was centered near –45° indicative of the majority of the vertical column stabilized by salinity. The Northwind Rise and Chukchi Plateau distributions were relatively wide implying more interleaving, while the Beaufort Sea and Mendelev Plain were relatively narrow with less interleaving. The vertical temperature structure of the Northwind Rise region and the Chukchi Plateau region possessed more interleaving and stronger double diffusive convection characteristics because the shear and internal wave activity associated with mesoscale features in these regions caused the increased lateral mixing of different water masses. In the Northwind Rise region the

Bering Sea Summer Water inflow was fragmented into numerous warm water intrusions; cold, salty intrusions were identified over the Chukchi Plateau region. The regional differences require multiple vertical profiles to accurately model the differences in vertical structure.

Bering Sea Summer Water inflow through the Bering Strait penetrated into the Canadian Basin interior in the form of warm water intrusions. The low molecular and double diffusive fluxes calculated for this area enable long-lived warm water intrusions to be an important mechanism for the lateral transport of heat at depths susceptible to entrainment into the mixed layer.

LIST OF REFERENCES

Aagaard, K., L. K. Coachman, and E. C. Carmack, On the Halocline of the Arctic Ocean, *Deep-Sea Res., Part A*, 28, 529-545, 1981.

Anderson, L. G., Chemical Oceanography of the Arctic and its Shelf Seas, in *Coastal and Estuarine Studies*. 49, American Geophysical Union, Washington, D. C.; 1995.

Carmack, E. C., Large-Scale Physical Oceanography of Polar Oceans.in Polar Oceanography, Part A: *Physical Science*, Walker O. Smith, Jr., Ed., Academic Press, Inc. New York, 171-222: 1990.

Carmack, E. C., K. Aagaard, J. H. Swift, R. W. MacDonald, F. A. McLaughlin, E. P. Jones, R. G. Perkin, J. N. Smith, K. M. Ellis, and L. R. Killius, Changes in Temperature and Tracer Distributions within the Arctic Ocean: Results from the 1994 Arctic Ocean Section, *Deep-Sea Res. II,* 44, 1487-1502, 1997.

Coachman, L. K., K. Aagaard, and R. B. Tripp, Bering Strait: The Regional Oceanography, University of Washington Press, Seattle; 1975.

Coachman, L. K., and C. A. Barnes, The Contribution of Bering Sea Water to the Arctic Ocean, *Arctic*, 14, 146- 161, 1961.

D'Asaro, E. A., Observations of Small Eddies in the Beaufort Sea, *J. Geophys. Res.*, 93, 6669-6684, 1988a.

D'Asaro, E. A., Generation of Submesoseale Vortices: A New Mechanism, *J. Geophys. Res.*, 93, 6685-6693, 1988b.

Environmental Working Group (EWG), *-Joint U.S.-Russian Atlas of the Arctic Ocean* [CD-ROM], Natl. Snow and Ice Data Cent., Boulder, CO, 1997.

Gill, A. E. Atmosphere-Ocean Dynamics Academic Press, Inc., New York; 1982.

Jones, E. P., D. M. Nelson, and P. Treguer, Large-Scale Physical Oceanography of Polar Oceans.in Polar Oceanography, Part B: Chemistry, Biology, and geology, Walker O. Smith, Jr., Ed., Academic Press, Inc., New York, 407-476; 1990.

Lide, D. R., ed. Handbook of Chemistry and Physics. 78th edition, CRC Press, Inc., New York; 1997.

Kundu, P. K., Fluid Mechanics, Academic Press, Inc., New York; 1990.

Maslowski, W. PIPS 3.0 web page [Available on-line from http;//www.oc.nps.navy.mil/~pips3], 2000.

McLaughlin, F. A., E. C. Carmack, R. W. Macdonald, and J.K.B. Bishop, Physical and Geochemical Properies Across the Atlantic/Pacific Water Mass Front in the Southern Canadian Basin, *J Geophys., Res.*, 101, 1183-1197, 1996.

Melling, H., Hydrographic Changes in the Canada Basin of the Arctic Ocean, 1979-1996, J. *Geophys. Res.*, 103, 7637-7645, 1998.

Melling, H., and E. L. Lewis, Shelf Drainage Flows in the Beaufort Sea and Their Effect on the Arctic Ocean Pycnocline, *Deep-Sea Res., 29,* 967-985, 1982.

Morison, J., M. Steele, and R. Anderson, Hydrography of the Upper Arctic Ocean Measured From the Nuclear Submarine U.S.S. Pargo, *Deep-Sea Res. I,* 45, 15-38, 1998.

Perovich, D. K., E. L. Andreas, J. A. Curry, H. Eiken, C. W. Fairall, T. C. Grenfell, P. S. Guest, J. Intrieri, D. Kadko, R. W. Lindsay, M. G. McPhee, J. Morison, R. E. Moritz, C. A. Paulson, W. S. Pegau, P. O. G. Persson, R. Pinkel, J. A. Richter-Menge, T. Stanton, H. Stern, M. Sturm, W. B. Tucker III, and T. Uttal, Year on Ice Gives Climate Insights, *EOS*, 80, 481-486, 1999.

Proshutinsky, A., M. Johnson, and I. Polyakov. Seasonal Variability for Two Climate Regimes. *AGU Fall Meeting*, San Francisco, CA, Amer. Geophys. Un., 1998.

Roach, A. T., K. Aagaard, C. H. Pease, S. A. Salo, T. Weingartner, V. Pavlov, and M. Kulakov, Direct Measurements of Transport and Water Properties Through the Bering Strait, , *J. Geophys. Res.*, 100, 18443-18457, 1995.

Ruddick, B. R., A Practical Indicator of the Stability of the Water Column to Double-Diffusive Activity, *Deep-Sea Res.*, 30, 1105-1107, 1983.

Ruddick, B. R., Intrusive Mixing in a Mediterranean Salt Lens – Intrusion Slopes and Dynamical Mechanisms, *J. Phys. Oceanogr.*, 22, 1274-1285, 1992.

Ruddick, B. R., and D. Walsh, Observations of the Density Perturbations which Drive Thermohaline Intrusions, in Double-Diffusive Convection, edited by Alan Brandt and H. J .S. Fernando, American Geophysical Union, Washington, D. C., 329-334, 1995.

Stanton, T. P., J. H. Morison, D.G. Martinson and R. D. Tyner, Upper Ocean Structure and Heat Content during the SHEBA Ice Camp Drift, *J. Geophys. Res.*, submitted 2000.

Steele, M., and T. Boyd, Retreat of the Cold Halocline Layer in the Arctic Ocean, *J. Geophys. Res.*, 103, 10419-10435, 1998.

Toole, J. M., and D. T. Georgi, On the Dynamics and Effects of Double-Diffusively Driven Intrusions, *Progress in Oceanography*, 10, 121-145, 1981.

Tyner, R. D., Decadal Variability of the Thermohaline Structure at the SHEBA Site, Masters Thesis, Naval Postgraduate School, Monterey, California, June 1999.

Turner, J. S., Double-diffusive Intrusions into a Density Gradient, *J. Geophys. Res.*, 83, 2887-2901, 1978.

Turner, J. S., Laboratory Models of Double-Diffusive Processes in Double-Diffusive Convection, edited by Alan Brandt and H. J .S. Fernando, American Geophysical Union, Washington, D. C., 11-29, 1995.

Walsh, J. E., E. P. Jones, W. L. Chapman, and T.L. Shy, Recent Decrease of Sea Level Pressure in the Central Arctic, *J. Climate*, 9, 480-486, 1996.

Weingartner, T. J., D. J. Cavalieri, K. Aagaard, and Y. Sasaki, Circulation, Dense Water Formation, and Outflow on the Northeast Chukchi Shelf, *J. Geophys. Res.*, 103, 7647-7661, 1998.

Williams, A. J., The Role of Double Diffusion in a Gulf Stream Frontal Intrusion, *J. Geophys. Res.*, 86, 1917-1929, 1981.

THIS PAGE INTENTIONALLY LEFT BLANK

INITIAL DISTRIBUTION LIST

1. Defense Technical Information Center 2
   8725 John J. Kingman Rd, STE 0944
   Ft. Belvoir, VA 22060-6218

2. Dudley Knox Library 2
   Naval Postgraduate School
   411 Dyer Rd
   Monterey, CA 93943-5101

3. Chairman (Code OC/Gd) 1
   Department of Oceanography
   Naval Postgraduate School
   Monterey, CA 93943-5122

4. Chairman (Code MR/Wx) 1
   Department of Meteorology
   Naval Postgraduate School
   Monterey, CA 93943-5114

5. Professor Tim Stanton, (Code OC/St) 2
   Department of Oceanography
   Naval Postgraduate School
   Monterey, CA 93943-5122

6. Dr. R. H. Bourke, (Code OC/Bf) 2
   Department of Oceanography
   Naval Postgraduate School
   Monterey, CA 93943-5122

7. Douglas Lamb 4
   14424 Burslem Terrace
   Burtonsville, MD 20866

8. Wendy Lamb 1
   3117 Stanhope Way
   Sacramento, CA 95833